

Article

Assessing the Impact of Groundwater Extraction on the Performance of Fractured Concrete Subsurface Dam in Controlling Seawater Intrusion in Coastal Aquifers

Asaad M. Armanuos ¹, Hossam E. Moghazy ², Martina Zeleňáková ^{3,*} and Zaher Mundher Yaseen ^{4,5}

¹ Irrigation and Hydraulics Engineering Department, Faculty of Engineering, Tanta University, Tanta 31733, Egypt; asaad.matter@f-eng.tanta.edu.eg

² Department of irrigation and Hydraulics, Faculty of Engineering, Alexandria University, Alexandria 21544, Egypt; hossam_moghazy@yahoo.com

³ Institute of Environmental Engineering, Faculty of Civil Engineering, Technical University of Košice, 04200 Košice, Slovakia

⁴ Department of Earth Sciences and Environment, Faculty of Science and Technology, Universiti Kebangsaan Malaysia, Bangi 43600, Selangor, Malaysia; yaseen@alayen.edu.iq

⁵ New Era and Development in Civil Engineering Research Group, Scientific Research Center, Al-Ayen University, Thi-Qar 64001, Iraq

* Correspondence: martina.zelenakova@tuke.sk

Abstract: Among the well-known approaches for controlling seawater intrusion during extensive freshwater abstraction from coastal aquifers is the construction of subsurface dams. In the current research, the SEAWAT code is being implemented to examine the impact of groundwater extraction on the effectiveness of a damaged subsurface dam for controlling saltwater intrusion. Simulations were performed numerically to check impact of the subsurface dam height, dam location, well height, well location, abstraction rate, fracture aperture, fracture location, seawater density and fracture dimension on the effectiveness of subsurface dam as a countermeasure to prevent saltwater intrusion in coastal aquifers. Increasing the abstraction rate from 1×10^{-6} to 5×10^{-6} m³/s caused the seawater to advance more into the freshwater, and the loss of effectiveness increased. The minimum and maximum value of loss of subsurface dam effectiveness was recorded to be 34.6% to 93%, respectively, for the abstraction rates from the well equal 1×10^{-6} and 5×10^{-6} m³/s, consequentially. When the dimensionless value of well height location L_w/L_d is increased from 1.0 to 2.0, the effectiveness of the subsurface dam is reduced by around 20%. The findings demonstrate that the well location, well depth, abstraction rate, location of the dam, fracture aperture, and density of saltwater all affect the effectiveness impairment of the fractured subsurface dam for controlling saltwater intrusion. Decision makers could use findings of this research to better manage groundwater resources in coastal aquifers.

Keywords: saltwater intrusion control; groundwater abstraction; concrete subsurface dam; fracture; abstraction well; loss of effectiveness; abstraction rate



Citation: Armanuos, A.M.; Moghazy, H.E.; Zeleňáková, M.; Yaseen, Z.M. Assessing the Impact of Groundwater Extraction on the Performance of Fractured Concrete Subsurface Dam in Controlling Seawater Intrusion in Coastal Aquifers. *Water* **2022**, *14*, 2139. <https://doi.org/10.3390/w14132139>

Academic Editor: Alexander Yakirevich

Received: 5 June 2022

Accepted: 29 June 2022

Published: 5 July 2022

Publisher's Note: MDPI stays neutral with regard to jurisdictional claims in published maps and institutional affiliations.



Copyright: © 2022 by the authors. Licensee MDPI, Basel, Switzerland. This article is an open access article distributed under the terms and conditions of the Creative Commons Attribution (CC BY) license (<https://creativecommons.org/licenses/by/4.0/>).

1. Introduction

Saltwater intrusion, or the pollution of coastal aquifers by oceanic seawater, has been a significant problem for coastal habitats in many regions all over the world, particularly because fresh groundwater resources are the most important sources of water supply [1]. In coastal areas, seawater intrusion (SWI) is the most significant limiting factor to groundwater extraction [2,3]. The seawater wedge continues to invade inland into coastal aquifers as a consequence of excessive groundwater extraction in coastal aquifers [4,5].

The current goal is to devise effective solutions for preventing saltwater intrusion, optimizing water extraction and preserving our resources of fresh groundwater [2,6]. Saltwater intrusion concerns have been addressed using a variety of control approaches.

Abd-Elhamid et al. [7] outline the most well-known approaches for controlling saltwater intrusion as follows: lowering the abstraction rate, pumping well relocation, subsurface groundwater barriers, artificial recharging, and seawater abstraction.

Through the study conducted by [1], the authors explored the effectiveness of cut-off walls for control seawater intrusion in stratified coastal aquifers using laboratory testing and the SEAWAT model. They combined the usage of cut-off walls and underground dams to improve the effectiveness of seawater intrusion prevention [8]. Luyun et al. [9] used laboratory testing and the SEAWAT model to investigate the relation between the underground dam's height and the seawater wedge thickness. Saltwater intrusion might be avoided, and the seawater retained upstream might be flushed out in case the subsurface dams remain higher than the seawater wedge thickness. Nevertheless, the consequences of subsurface dam construction locations and the groundwater head differences were overlooked. The depth of a wall, the hydraulic conductivity, the distance from the shore, the velocity of the groundwater, the heterogeneity, and the anisotropy are all factors that influence the effectiveness of underground dams in avoiding SWI [10].

Anwar [11] proposed an analytical relation for determining the position of the seawater interface when a cutoff wall was implemented, with the coefficients established from laboratory experimentation. Luyun et al. [12] evaluated the impact of cutoff wall locations and depth on cutoff wall effectiveness. They came to the conclusion that the performance of cutoff walls increases when they are positioned deeper and nearer to the coastline, as long as they are inside the original saltwater wedge area.

The study conducted by [1] recommended the mixed physical barrier (MPB), which combines a cutoff wall with a semi-permeable underground dam. This approach generated a significant decrease in seawater length by promoting the upwards uplifting of saltwater towards to the coastline. Armanuos et al. [13] evaluated the influence of a barrier wall, recharging through a well, and a combination of these to limit saltwater intrusion in coastal aquifers using experimental tests and SEAWAT numerical simulation. The influence of the wall depth ratio and the freshwater injection rate on the decrease in saltwater penetration wedge length was investigated by the authors.

Chang et al. [14] described experimental tests and the numerical assessment of an underground dam's effectiveness in controlling saltwater intrusion. To investigate the impacts of underground dam height, distance from the seashore line, groundwater head variations, and the fresh groundwater outflow, the authors conducted a series of lab experiments and SEAWAT simulations. In sloping unconfined coastal aquifers, Armanuos et al. [15] studied the impacts of using a flow barrier to control saltwater intrusion. The authors utilized the SEAWAT program to simulate the barrier's effectiveness in controlling seawater intrusion. The repulsion ratio increases as the barrier depth increases, according to the authors. Decision-makers can use the results of this research as a management strategy for coastal aquifers. SEAWAT was used by Armanuos et al. [16] to investigate the impact of employing freshwater recharge from wells for reducing saltwater intrusion in sloped coastal aquifers. The impact of modifying the slope of aquifer bed and hydraulic variables on the saltwater intrusion repulsion ratio was examined using a sensitivity analysis. The outcomes showed that injections in the toe location resulted in increased repulsion ratios.

In shallow, unconsolidated, and unconfined coastal aquifers, Ebeling et al. [17] examined the performance of the mixed hydraulic barrier technique for the remediation of SWI. Decreased inland pumping of supply wells and positive barrier injection rates provide the greatest remediation impacts, according to the findings. Installing the positive barrier inside the saltwater wedge, on the other hand, runs the danger of trapping salt on the landside. As a result, this research demonstrates that mixed hydraulic barrier remediation is viable when carried out in accordance with local conditions.

Ozaki et al. [18] tested the effectiveness of a barrier well on the probable freshwater discharge from a producing well on a lab scale. In addition, the authors assessed the experimental data; a 2D numerical model was built and simulated using the similar characteristics as those employed in the tests. When the abstraction ratio was smaller

than the critical ratio, a saltwater upcoming of seawater concentration towards the barrier well was detected in the numerical simulation.

Recently, Laabidi et al. [19] utilized FEFLOW to assess the influence of fractures in concrete cutoff walls on the loss of the effectiveness of concrete cutoff walls used to prevent saltwater intrusion in coastal groundwater aquifers. The penetration lengths of the saltwater intrusion wedge after fracture were compared to the base Henry case to evaluate the performance of fractured cutoff walls. The results confirmed that the effectiveness of a fractured cutoff wall is more sensitive for the fracture aperture, the height of the aperture, and the saltwater density. The motivation of the current study was initiated from the concept of groundwater sustainability and management [20,21]. Having an appropriate management for groundwater environments is an essential aspect for avoiding marine and oceanology infrastructure [22].

In this study, the SEAWAT code is used to assess the impact of groundwater extraction on the performance of a fractured concrete subsurface dam in controlling saltwater intrusion in coastal aquifers. The penetration length of the saltwater wedge after installing a subsurface dam and adjusting the groundwater abstraction from the groundwater well were compared to the base scenario case of the Henry seawater intrusion problem.

2. Materials and Methods

The finite difference code SEAWAT (Guo and Langevin (2002) was used to examine the impact of groundwater extraction on the performance of a fractured concrete subsurface dam in controlling seawater intrusion in coastal aquifers. Furthermore, the impact of a fractured concrete subsurface dam was simulated using Henry's problem configurations with the same hydrodynamic parameters and boundary conditions of freshwater and saltwater to offer significant general conclusions (Henry 1964). Table 1 lists the values of input parameters of the SEAWAT code for the Henry saltwater problem employed in numerical simulations. For the numerical simulation of seawater intrusion, the SEAWAT code has been extensively used. SEAWAT is a code that links MODFLOW and MT3DMS together. The code is implemented for solving the linked groundwater flow and the pollutant transport equations. The variable density groundwater flow computations are utilized by the SEAWAT code. In this research, the dimensions of the Henry saltwater problem were employed to investigate the impact of freshwater extraction on the effectiveness of a fractured subsurface dam.

The created model domain has dimensions of 200 cm in the horizontal coordinate and 100 cm in the vertical coordinate. The cell sizes were adjusted to be $\Delta x = \Delta y = 2.0$ cm. The dispersivity values in the longitudinal and transverse directions were adjusted to 1 and 0.1 mm, respectively, for all simulated instances. The freshwater flux boundary, in the freshwater side, was set to 6.6×10^{-5} m/s, while the saltwater head (h_s) in the sea side was set at 100 cm. In the saltwater boundary, the density of saltwater was set at 1025 kg/m^3 , with a total dissolved concentration (salinity concentration) of 35,000 mg/L. The density of freshwater in the freshwater boundary was set to 1000 kg/m^3 , and the freshwater had a total dissolved concentration (salinity concentration) of 0.0 mg/L. The initial salinity concentration of the porous aquifer media was set at 0.0 mg/L. Because the aquifer was assumed to be homogeneous and isotropic, the value of the hydraulic conductivity for the aquifer system was 0.01 m/s in the x, y, and z directions. It had a porosity of 0.35. Table 1 shows the problem parameter specifications as well as numerical simulations.

The SEAWAT model was run for three periods: firstly in the steady-state condition, and secondly and thirdly in the transient state. In the second period, the fracture in the concrete subsurface dam was adjusted after the steady-state of the saltwater intrusion wedge was reached. The saltwater behind the dam flows through the fracture opening in the fracture subsurface dam. After the seawater intrusion wedge reached steady-state in the second period, different abstraction rates from groundwater wells were tested to study the impact of groundwater extraction on the effectiveness of fractured underground dams in preventing and controlling saline intrusion in coastal aquifers.

Table 1. Numerical simulation parameters.

Symbol	Definition	Value	Unit
L	Length of the domain	2.0	m
d	Depth of the domain	1.0	m
n	Aquifer porosity	0.35	–
k	The value of hydraulic conductivity	0.01	m/s
d_0	Molecular diffusion coefficient	6.6×10^{-6}	m^2/s
q_b	Freshwater flux boundary	6.6×10^{-5}	m/s
ρ_f	Density of freshwater	1000	Kg/m^3
ρ_s	Density of saltwater	1025	Kg/m^3
C_S	Saltwater concentration	35,000	mg/L
C_f	Freshwater concentration	0.0	mg/L
α_l	Longitudinal dispersivity coefficient	0.0	m
α_t	Transversal dispersivity coefficient	0.0	m
μ	Fluid viscosity	1×10^{-3}	$Kg/m.s$
g	Gravity acceleration	9.81	m/s^2
Δx	Cell dimension in horizontal direction	0.02	m
Δz	Cell dimension in vertical direction	0.02	m
L_d	Dam position from the sea boundary	0.30, 0.50	m
L_d/L	Dam location ratio	0.3/2, 0.5/2	–
H_d	Dam height	0.5, 0.6, 0.7, 0.8	m
L_w	Well location	0.15, 0.30, 0.50, 1.0	m
H_w	Well height	0.15, 0.30, 0.45, 0.60	m
L_w/L_d	Well location ratio	1.0, 2.0	–
H_w/H_d	Well height ratio	0.25, 0.50, 0.75, 1.0	–

2.1. Investigated Configurations

In addition to resistance, a concrete structure should serve structural functions. In this setting, reinforced concrete cracking is critical to the structure's longevity, waterproofing, and stability. Fracturing, cracking, scaling, weathering, and spalling are common symptoms of damage to a concrete structure (Figure 1). According to [23], those fractures and cracks might be in the horizontal direction or oblique. These damages can be caused by a variety of factors, the most common of which are:

- **Carbonation:** Whenever carbon dioxide passes via microcracks and pores in concrete, it combines with hydroxides such as calcium hydroxide to generate calcium carbonate. The reaction's result lowers the pH of the concrete from 13 to 8. Embedded steel reinforcement bars are exposed to corrosion as the alkalinity decreases. Carbonation, on the other hand, has no impact on the deterioration speed of steel bars.
- **Reinforcement Corrosion:** Concrete failure is frequently caused by the corrosion of the steel reinforcement. It happens when the pH of the concrete falls below 10, allowing chloride ions, oxygen, and moisture to enter. As a consequence, the corrosion product volume (rust) produced exceeds that of steel, causing the surrounding concrete to fracture, delaminate, or spall off. Corrosion of embedded reinforcement in concrete can be considerably reduced by using concrete with low permeability and no cracks, as well as providing enough concrete cover above steel bars.
- **Chemical Attack:** Sulfates of sodium, potassium, calcium, or magnesium dissolved in soil, groundwater, or saltwater can infiltrate concrete, react with hydrated substances, and expand, causing damage to the concrete structure. Internal sulphate attack also produces a substance that causes the absorption of water and produces substantial swelling and cracking of concrete.
- **Overloading and Impacts:** Microcracks and cracks appear when significant loads are placed on concrete. Overloading can also develop as a result of variations in the building's functioning without sufficient structural modifications, unintentional overload, and uncommon events such as earthquakes.
- **Fire Damage:** Concrete loses most of its compressive strength, flexural strength, and elasticity when subjected to a higher heat. Consequently, concrete with a high

aggregate-to-cement ration loses less compressive strength, and the smaller the water-to-cement ratio, the less elastic modulus is lost. Spalling of concrete can occur as a consequence of existence trapped water.

- Over-Wet Concrete: The presence of a lot of water in the concrete mix causes the cement to rise to the top. As a consequence, the concrete surface will dry out before it sets, resulting in shrinkage, cracks, laitance, and a decrease in the compressive strength of concrete.

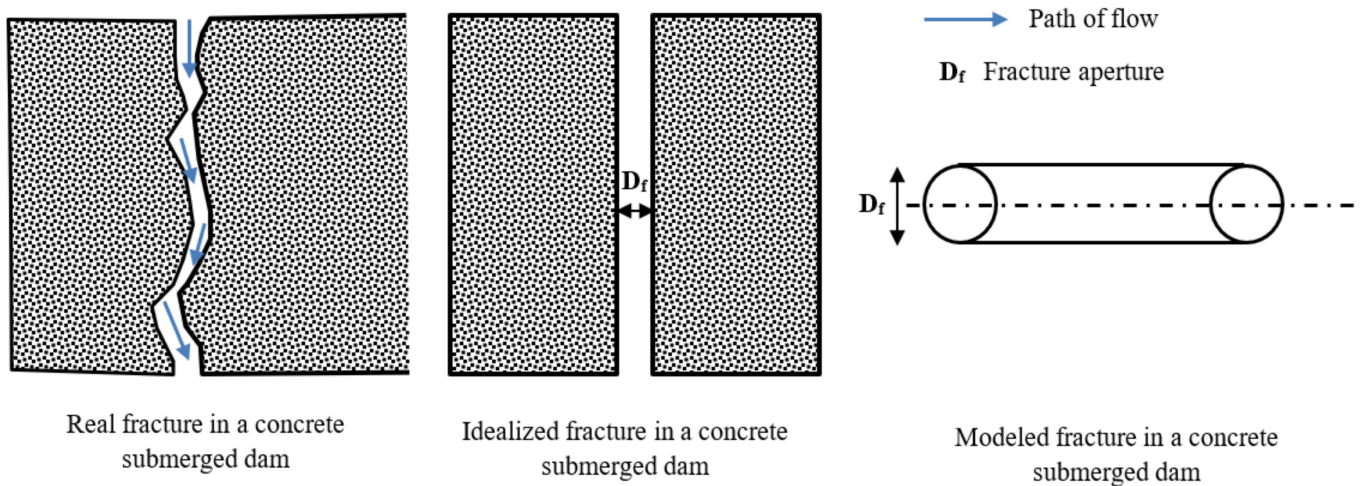


Figure 1. Real, idealized, and modeled fracture shapes in a concrete subsurface dam [24].

2.2. Sensitivity Analysis

To evaluate the impact of groundwater abstraction on the penetration length of saltwater intrusion and evaluate the performance of a fractured concrete subsurface dam in controlling saltwater intrusion in coastal aquifers, a sensitivity analysis was conducted utilizing the exact geometric properties of the Henry seawater problem (Figure 2).

The tested parameters are: the abstraction rate of freshwater from the aquifer, the well height ratio, the well location ratio, the location of the subsurface dam, the height of subsurface dam, the fracture aperture, the height of fracture aperture, and the density of saltwater.

Table A1 in Appendix A presents the important variables employed in the sensitivity investigation simulations, as shown in Figure 2. The penetration length of saltwater intrusion of the base reference case of the Henry seawater problem is employed in the presented tested numerical simulations (Table A1).

The loss of saltwater penetration reduction (the loss of subsurface dam effectiveness), as a percentage, due to the freshwater abstraction for the fractured subsurface dam is equal to the difference of $RE_{afw/0} - RE_{w/0}$. The loss of subsurface dam effectiveness is equal to the difference between the decrease in the saltwater penetration percentage due to freshwater abstraction ($RE_{afw/0}$) and the decrease in the saltwater penetration percentage due to the subsurface dam construction ($RE_{w/0}$). The $RE_{w/0}$ is the percentage decrease in saltwater penetration due to the subsurface dam construction compared with the base scenario case of the Henry problem $(L_{toe0} - L_{toew})/L_{toe0}$. The $RE_{afw/0}$ is the percentage of saltwater penetration due to the abstraction of freshwater for the fractured subsurface dam compared to the base case $(L_{toe0} - L_{toefw})/L_{toe0}$, where the parameters L_{toe0} , L_{toew} , and L_{toefw} refer to the penetration length of seawater intrusion wedge for the base case, after subsurface dam construction, and after freshwater abstraction for fractured subsurface dam, respectively.

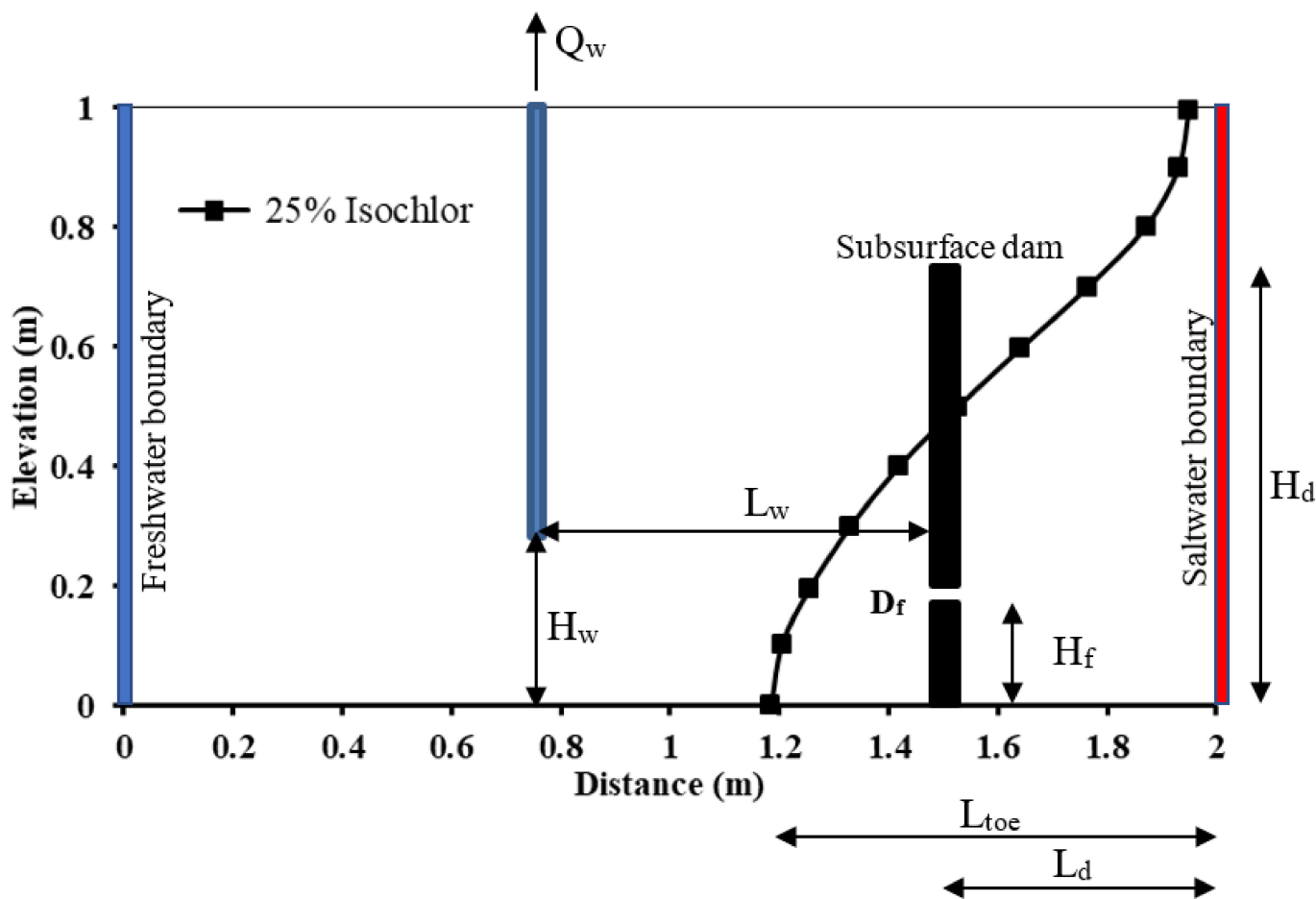


Figure 2. Schematic diagram of the simulated numerical configurations and the main key problem variables.

The simulation of seawater intrusion was repeated for four different positions of a groundwater well in order to detect the impact of location of groundwater abstraction point on the advancement of seawater intrusion wedge. The well height (H_w) measured from the bottom of the aquifer was 0.15, 0.30, 0.45, and 0.60 m, with dimensionless well height ratios (H_w/H_d) equal to 0.25, 0.50, 0.75, and 1.0, respectively. The simulations were tested for two various distances of the groundwater well (L_w) with dimensionless location ratios (L_w/L_d) equal to 0.50 and 1.0. Four different underground dam heights (H_d) were adjusted in the numerical simulations equal to 50, 60, 70, and 80 cm measured from the bottom of the aquifer. Two different underground dam positions (L_d) equal to 0.30 and 0.50 m measured from the sea boundary were included in the numerical runs. The fracture height (H_f) was changed in the numerical simulations to be 0.10 m and 0.20 m in order to test the impact of fracture location on the intrusion of seawater. Five different abstraction rate values from the groundwater well (Q_w) were tested equal to 1×10^{-6} , 2×10^{-6} , 3×10^{-6} , 4×10^{-6} , and 5×10^{-6} m³/s. Two different configurations of the fracture aperture were tested with fracture diameters (D_f) equal to 0.005 m and 0.01 m. Four different saltwater density values were implemented in numerical tests equal to 1022, 1025, 1027, and 1030 kg/m³, with corresponding saltwater concentrations equal to 30,000, 35,000, 37,500, and 40,000 mg/L, respectively. A sensitivity analysis was performed through groups of simulations in order to study the effectiveness of variations in well location, well distance, saltwater density, saltwater concentration, underground dam height, underground dam location, and fracture aperture on the achieved repulsion ratio of seawater intrusion through fractured concrete subsurface dams.

2.3. Dimensional Analysis

The dimensional analysis for the current study can be expressed as follows:

$$\emptyset(R, K, H, H_d, L_d, H_w, L_w, Q_w, D_f, H_f, \rho_s, \rho_f, g, n, C_s, C_f, v_s, v_f, \alpha_L, \alpha_T) = 0.0$$

The number of variables = 20, the number of repeated dimensions = 3, and the number of $\pi = 17$

Select H, K, and ρ_s :

$$\emptyset(\pi_1, \pi_2, \pi_3, \pi_4, \pi_5, \pi_6, \pi_7, \pi_8, \pi_9, \pi_{10}, \pi_{11}, \pi_{12}, \pi_{13}, \pi_{14}, \pi_{15}, \pi_{16}, \pi_{17}, \pi_{18}) = 0.0$$

$$\emptyset\left(R, \frac{H_d}{H}, \frac{L_d}{H}, \frac{H_w}{H}, \frac{L_w}{H}, \frac{Q_w}{H^2K}, \frac{D_f}{H}, \frac{H_f}{H}, \frac{\rho_f}{\rho_s}, n, \frac{C_s}{\rho_s}, \frac{C_f}{\rho_s}, \frac{v_s}{HK}, \frac{v_f}{HK}, \alpha_L, \alpha_T\right) = 0.0$$

In the current study, we consider k, H, g, n, α_L , α_T , v_s , v_f , C_s , and C_f to be constant.

To study the effect of subsurface dam distance L_d , π_3 is divided by π_2 .

To study the combined effect of groundwater well height H_w and subsurface dam height H_d , π_4 is divided by π_2 .

To study the combined effect of well distance and subsurface dam distance d_2 , π_5 is divided by π_3 .

To study the effect of fracture aperture, π_7 is divided by π_2 .

To study the effect of fracture location, π_8 is divided by π_2 .

Accordingly, we can obtain the following function for the repulsion ratio of seawater intrusion wedge length:

$$R = f\left(\frac{H_d}{H}, \frac{L_d}{H_d}, \frac{H_w}{H_d}, \frac{L_w}{L_d}, \frac{Q_w}{H^2K}, \frac{D_f}{H_d}, \frac{H_f}{H_d}, \frac{\rho_f}{\rho_s}\right)$$

3. Governing Equations

3.1. Governing Equation for Flow

With the explanation of the freshwater head and Darcy’s law in relation to freshwater head, the describing equation for ground-water flow can be expressed in phrases of equivalent freshwater head.

The following equation is the governing equation for the variable-density flow in phrases of freshwater head as utilized in SEAWAT:

$$\begin{aligned} \frac{\partial}{\partial \alpha} \left(\rho K_{f\alpha} \left[\frac{\partial h_f}{\partial \alpha} + \frac{\rho - \rho_f}{\rho_f} \frac{\partial Z}{\partial \alpha} \right] \right) + \frac{\partial}{\partial \beta} \left(\rho K_{f\beta} \left[\frac{\partial h_f}{\partial \beta} + \frac{\rho - \rho_f}{\rho_f} \frac{\partial Z}{\partial \beta} \right] \right) + \frac{\partial}{\partial \gamma} \left(\rho K_{f\gamma} \left[\frac{\partial h_f}{\partial \gamma} + \frac{\rho - \rho_f}{\rho_f} \frac{\partial Z}{\partial \gamma} \right] \right) \\ = \rho S_p \frac{\partial h_f}{\partial t} + \theta \frac{\partial \rho}{\partial C} \frac{\partial C}{\partial t} - \bar{\rho} q_s \end{aligned}$$

where:

h_f is the freshwater head;

$K_{f\alpha}$ is the freshwater hydraulic conductivity in the α direction;

$K_{f\beta}$ is the freshwater hydraulic conductivity in the β direction;

$K_{f\gamma}$ is the freshwater hydraulic conductivity in the γ direction;

θ is the porosity value;

$S_f [L^{-1}]$ is the volume of water rescued from storage in a unit volume of the aquifer per unit drop in the freshwater head;

S_p is the specific storage in phrases of pressure;

Z is the elevation above the datum;

t is the time;

ρ is the density of saline water $[ML^{-3}]$;

ρ_f is the density of freshwater $[ML^{-3}]$;

$\bar{\rho}$ is the density of water inflowing from a source or escaping through a sink $[ML^{-3}]$.

3.2. Governing Equation for Solute Transport

Advection, molecular diffusion, and mechanical dispersion all contribute to the transfer of solute volume in porous materials. The following equation [25] can be utilized to explain the solute transport in ground water:

$$\frac{dC}{dt} = \nabla \times (D \times \nabla C) - \nabla \times (\vec{v}C) - \frac{q_s}{\theta} C_s + \sum_{k=1}^N R_k$$

where:

D is the coefficient of hydrodynamic dispersion (L^2T^{-1});

\vec{v} is the fluid velocity;

C_s is the solute concentration of water coming from sources or sinks (ML^{-3});

R_k is the rate of solute concentration or decay in reaction k of N various reactions ($ML^{-3}T^{-1}$);

∇ is the gradient operator;

q_s is the volumetric flow rate per unit volume of aquifer-representative sources and sinks [T^{-1}].

Binet et al. [26] uses a 2D equivalent porous medium to examine the exchanges between a conduit network and a solid matrix. The conduit was modelled as a discrete element in which Manning–Strickler’s law was used to compute flows. The Manning–Strickler law was shown to be suitable for describing flows in fractured and karstic conduits.

The Darcian velocity equation’s conductivity tensor K_{ij} can be interpreted as a basic Darcy law, Hagen Poiseuille law, or Manning–Strickler law [27].

The fracture discharge Q_c [L^3T^{-1}] could be expressed utilizing a 1D Manning–Strickler law as follows:

$$Q_c = -A_c \cdot f \cdot r^{\frac{2}{3}} \cdot \sqrt{\frac{dh}{dx}}$$

where:

dh/dx is the head loss in the fracture at the x -coordinate [dimensionless], r is the fracture hydraulic radius [L], f is the coefficient of friction [$L^{1/3}T^{-1}$], and A_c is the fracture area [L^2].

4. Results and Discussion

4.1. Model Calibration

Figure 3 presents the saltwater intrusion wedge for the Henry problem using a semi-analytical solution and the SEAWAT code. The comparison between the two figures confirmed good agreement for the concentration of 17,500 mg/L (50% Isochlor) and the salinity concentration of 7850 mg/L (25% Isochlor). The penetration of seawater intrusion for the salinity concentration of 17,500 mg/L is equal to 63 cm and 65.7 cm for the semi-analytical and SEAWAT code solutions, respectively. In addition, the penetration of seawater intrusion for the salinity concentration of 7850 mg/L is equal to 84.7 cm and 81.5 cm for the semi-analytical and SEAWAT code solutions, respectively. The absolute error of the penetration length of the seawater wedge between the semi-analytical solution and the SEAWAT code is equal to 2.7 cm and 3.2 cm for salinity concentrations of 17,500 and 7850 mg/L, respectively.

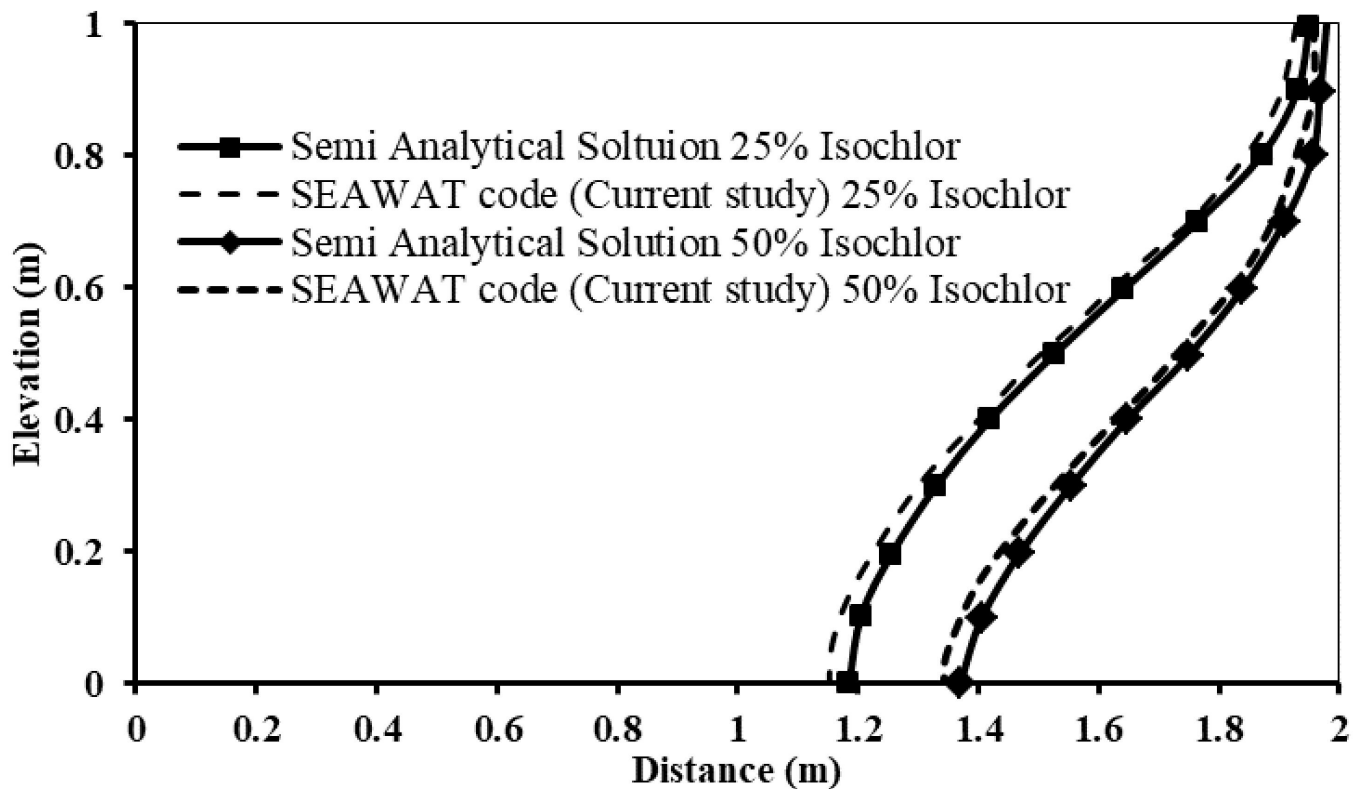


Figure 3. Comparison between saltwater intrusion wedge for SEAWAT code and the semi-analytical solution of the Henry saltwater problem.

Figure 4a,b shows the saltwater intrusion wedge of the Henry saltwater problem for the steady-state condition and after installing a subsurface dam with a height $H_d = 0.60$ m to control seawater intrusion at distance $L_d = 0.50$ m. Figure 4c–g present the saltwater intrusion wedges for a fractured subsurface dam with $D_f = 0.005$ m at a height $H_f = 0.1$ m and for five different well abstraction rates from equal to 1×10^{-6} , 2×10^{-6} , 3×10^{-6} , 4×10^{-6} , and 5×10^{-6} m^3/s , respectively.

The penetration length of the saltwater wedge in the Henry problem for steady-state condition is equal to 84.7 cm ($L_{\text{toe}0}$); the length of the saltwater intrusion toe is reduced to 50 cm after installing a subsurface dam at a distance of 50 cm from the seaside (L_{toew}). The penetration lengths of the saltwater wedge are equal 76, 87, 99, 111, and 125 cm, measured from the sea side for well abstraction rates of 1×10^{-6} , 2×10^{-6} , 3×10^{-6} , 4×10^{-6} , and 5×10^{-6} m^3/s , respectively (L_{toefw}). The loss of effectiveness increased with the increasing well abstraction rate.

The saltwater penetration percentage decreased as a result of the subsurface dam's construction compared to the base scenario of the Henry problem equal to 40.9% ($RE_{w/0}$).

The saltwater penetration percentage decreased because of the abstraction of freshwater for the fractured subsurface dam compared to the base cases of 10.27, -2.71 , -16.88 , -31.05 , and -47.5% ($RE_{\text{afw}/0}$). The loss of subsurface dam effectiveness was equal to 30.69%, 43.68%, 57.85%, 72.02%, and 88.54% for well abstraction rates of 1×10^{-6} , 2×10^{-6} , 3×10^{-6} , 4×10^{-6} , and 5×10^{-6} m^3/s , respectively.

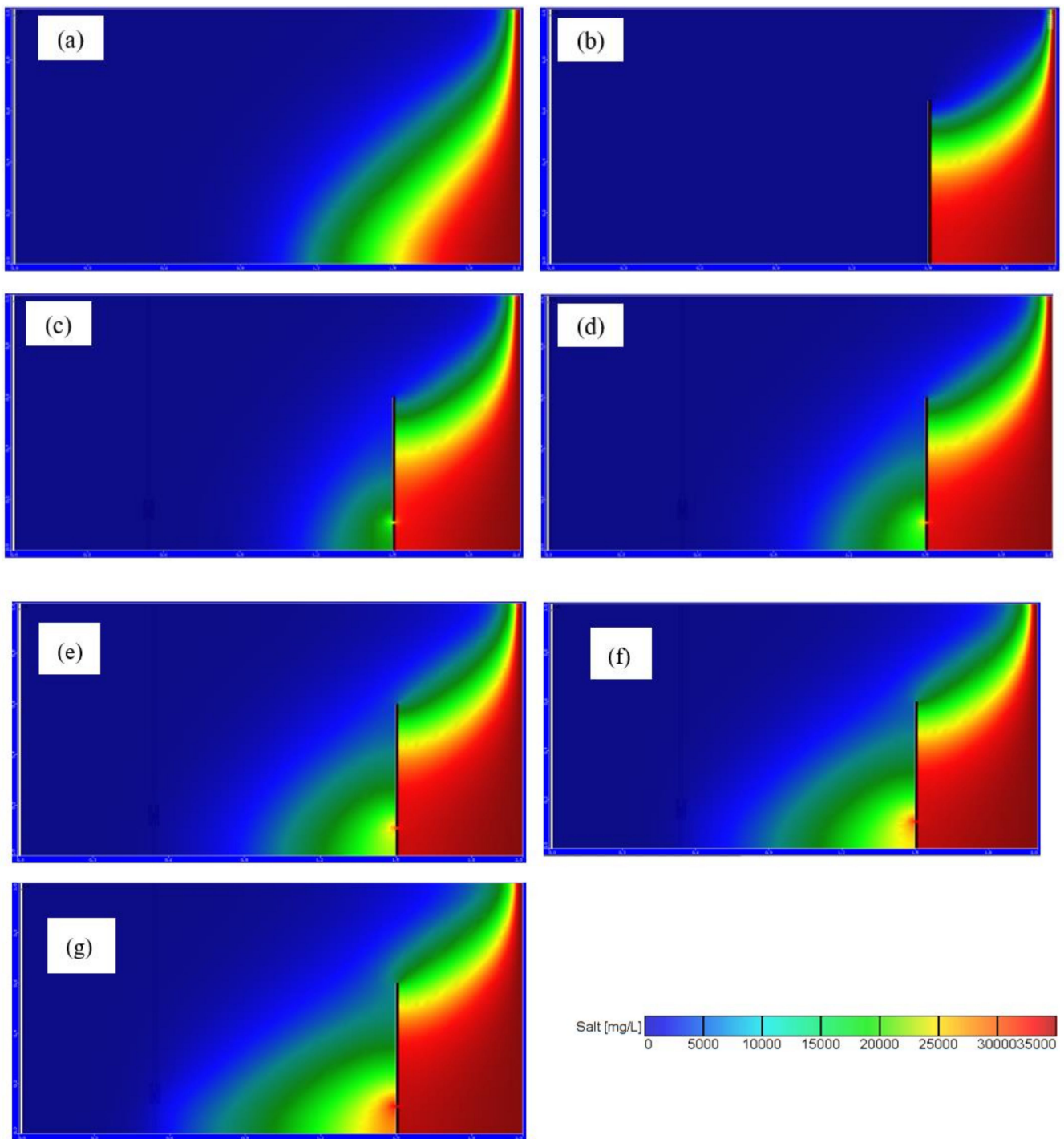


Figure 4. Steady-state saltwater intrusion for: (a) Henry base case; (b) subsurface dam at $L_d = 0.5$ m with $H_d = 0.6$ m; (c) $D_f = 0.005$ m, $H_f = 0.1$ m, $Q_w = 1 \times 10^{-6} \text{ m}^3/\text{s}$; (d) $D_f = 0.005$ m, $H_f = 0.1$ m, $Q_w = 2 \times 10^{-6} \text{ m}^3/\text{s}$; (e) $D_f = 0.005$ m, $H_f = 0.1$ m, $Q_w = 3 \times 10^{-6} \text{ m}^3/\text{s}$; (f) $D_f = 0.005$ m, $H_f = 0.1$ m, $Q_w = 4 \times 10^{-6} \text{ m}^3/\text{s}$; and (g,d) $D_f = 0.005$ m, $H_f = 0.1$ m, $Q_w = 5 \times 10^{-6} \text{ m}^3/\text{s}$.

4.2. Impact of Extraction Well Rate on the Loss of Effectiveness of Subsurface Dam to Control Seawater Intrusion

All numerical simulations used to examine the impact of the well abstraction rate on the loss of effectiveness of the subsurface dam were performed for $L_d = 0.5$ m for two values of $L_w/L_d = 1.0$ and 2.0 and for two values of $D_f = 0.005$ and 0.01 m. Five different abstraction rates were tested, ranging from 1×10^{-6} to 5×10^{-6} m^3/s . In all of the simulated situations, increasing the well extraction rate resulted in a greater loss of subsurface dam effectiveness.

Figure 5 depicts the relation between the loss of effectiveness of the subsurface dam and the rate of abstraction for different well location ratios H_w/H_d 0.25, 0.50, 0.75, and 1.0 for two different values of $L_w/L_d = 1.0$ and 2.0 and for two different values of H_f equal to 0.1 and 0.2. As presented in Figure 5a,b, increasing the abstraction rate from 1×10^{-6} to 5×10^{-6} m^3/s caused the seawater to advance more into the freshwater and the loss of effectiveness to increase. The percentage of loss increased from 31.1% to 69.6% for the case of $D_f = 0.005$, 0.01 m and for $L_w/L_d = 1.0$; in addition, it increased from 29.9% to 89.7% for the case of $L_w/L_d = 2.0$. The maximum loss of effectiveness was recorded for $L_w/L_d = 2.0$, $D_f = 0.005$. On the other hand, the minimum percentage of loss for subsurface dam effectiveness was recorded at $L_w/L_d = 2.0$, $D_f = 0.005$ and is approximately equal to 29.9% for an abstraction rate of 1×10^{-6} m^3/s and $H_w/H_d = 0.25$. In addition, the findings of figs. 5c and 5d revealed that, in addition to the increased abstraction rate, the loss of affectivity increases. The values of subsurface dam loss effectiveness were recorded to be less than the case of fracture height H_f equals 0.1 m. The loss of effectiveness increased dramatically from 7.17% to 62.2% for $H_w/H_d = 0.25$, $L_w/L_d = 1.0$, and for $D_f = 0.005$ m for abstraction rates equal to 1×10^{-6} and 5×10^{-6} m^3/s , respectively. In addition, for $L_w/L_d = 1.0$, the loss of effectiveness increased gradually from 2.39% to 81.34% for the same conditions of well location, height, and abstraction rate.

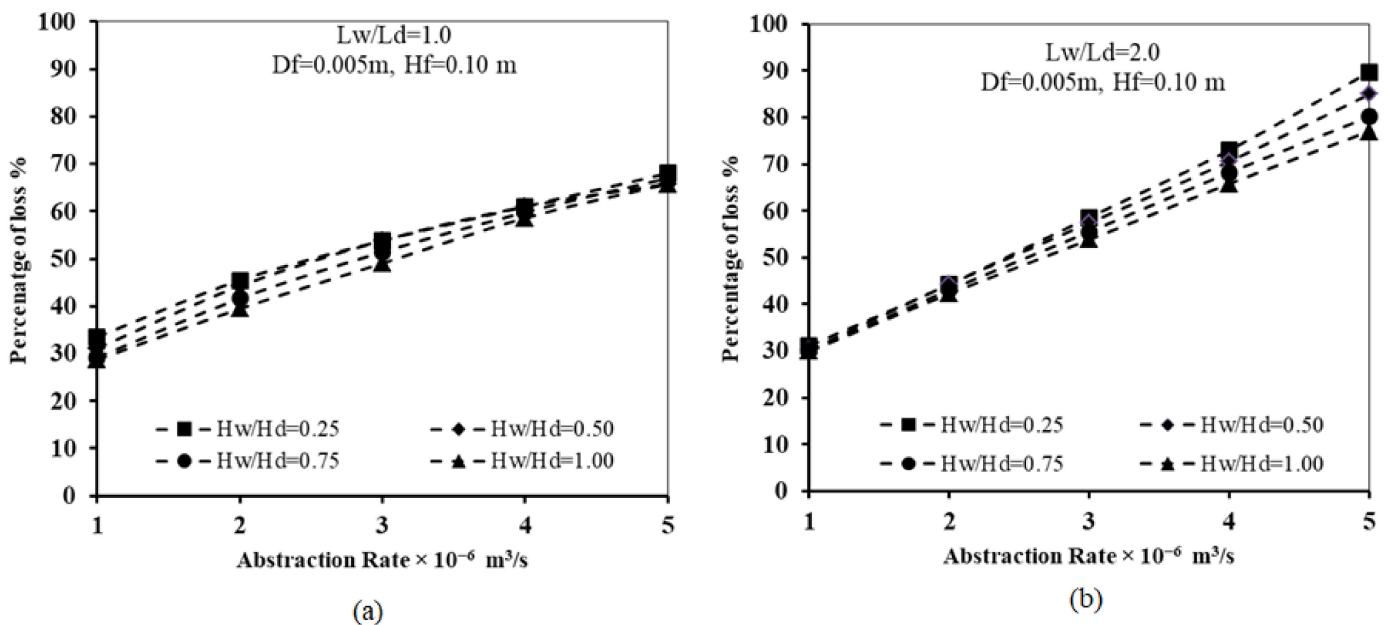


Figure 5. Cont.

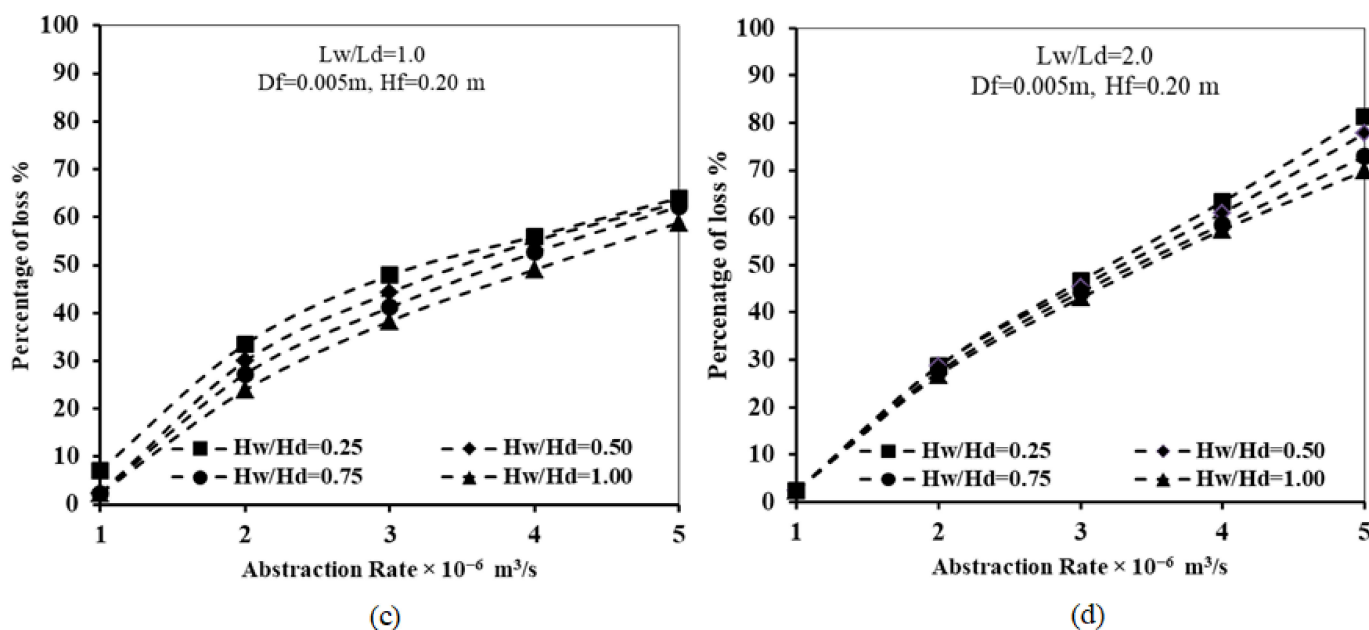


Figure 5. Relation between abstraction well rate and loss of subsurface dam effectiveness for $L_d = 0.50$ m, $D_f = 0.005$ m and for different L_w/L_d and H_f : (a) $L_w/L_d = 1.0$ and $H_f = 0.1$, (b) $L_w/L_d = 2.0$ and $H_f = 0.1$, (c) $L_w/L_d = 1.0$ and $H_f = 0.2$, and (d) $L_w/L_d = 2.0$ and $H_f = 0.2$.

Figure 6 demonstrates the same results of Figure 5 but for $D_f = 0.01$ m. The loss of effectiveness of the subsurface dam gradually increased as the abstraction rate was increased from 1×10^{-6} to 5×10^{-6} m³/s for all simulated well height ratios H_w/H_d and for the two well location ratios L_w/L_d . The loss of subsurface dam effectiveness was increased gradually from 38.2% to 71.8% and from 34.7% to 93% for L_w/L_d equal 1.0 and 2.0, respectively, for the same conditions of fracture aperture, fracture height, and subsurface dam height (Figure 6a,b). When the value of L_w/L_d is increased from 1.0 to 2.0, the value of loss of effectiveness increases by around 21.25 percent. The minimum and maximum values of loss of subsurface dam effectiveness were recorded to be 34.6% to 93%, respectively, for well abstraction rates equal to 1×10^{-6} and 5×10^{-6} m³/s (Figure 6a,b). As presented in figs. 6c and 6d, the maximum values of loss of subsurface dam effectiveness were observed for $H_w/H_d = 0.25$; the maximum value increased gradually from 14.35% to 65.7% and from 10.8% to 90.9% for $L_w/L_d = 1.0$ and 2.0, respectively. The minimum loss of effectiveness was below 11% for the lowest abstraction rate, 1×10^{-6} m³/s, for the four different values of H_w/H_d .

It can be concluded from the results of Figures 5 and 6 that increasing the rate of abstraction of groundwater well has a significant impact on reducing the performance of fractured subsurface dam in controlling seawater intrusion. The volume of transported seawater, behind the dam, from the opening of fracture in the subsurface dam increased with the increase in the groundwater abstraction rate. As a result, the area of the seawater wedge increased, the penetration length of seawater increased, and, in contrast, the effectiveness of the subsurface dam in preventing seawater intrusion decreased. It can be concluded from the findings of Figures 5 and 6 that positioning the groundwater well far away from the underground dam forced a large amount of saltwater to travel through the fracture aperture in the subsurface dam and move downstream the dam until reaching the screen of the groundwater well. As a result, the penetration length of the seawater intrusion increased when installing the groundwater well away from the location of the underground dam. In addition, the loss of subsurface dam effectiveness was reduced.

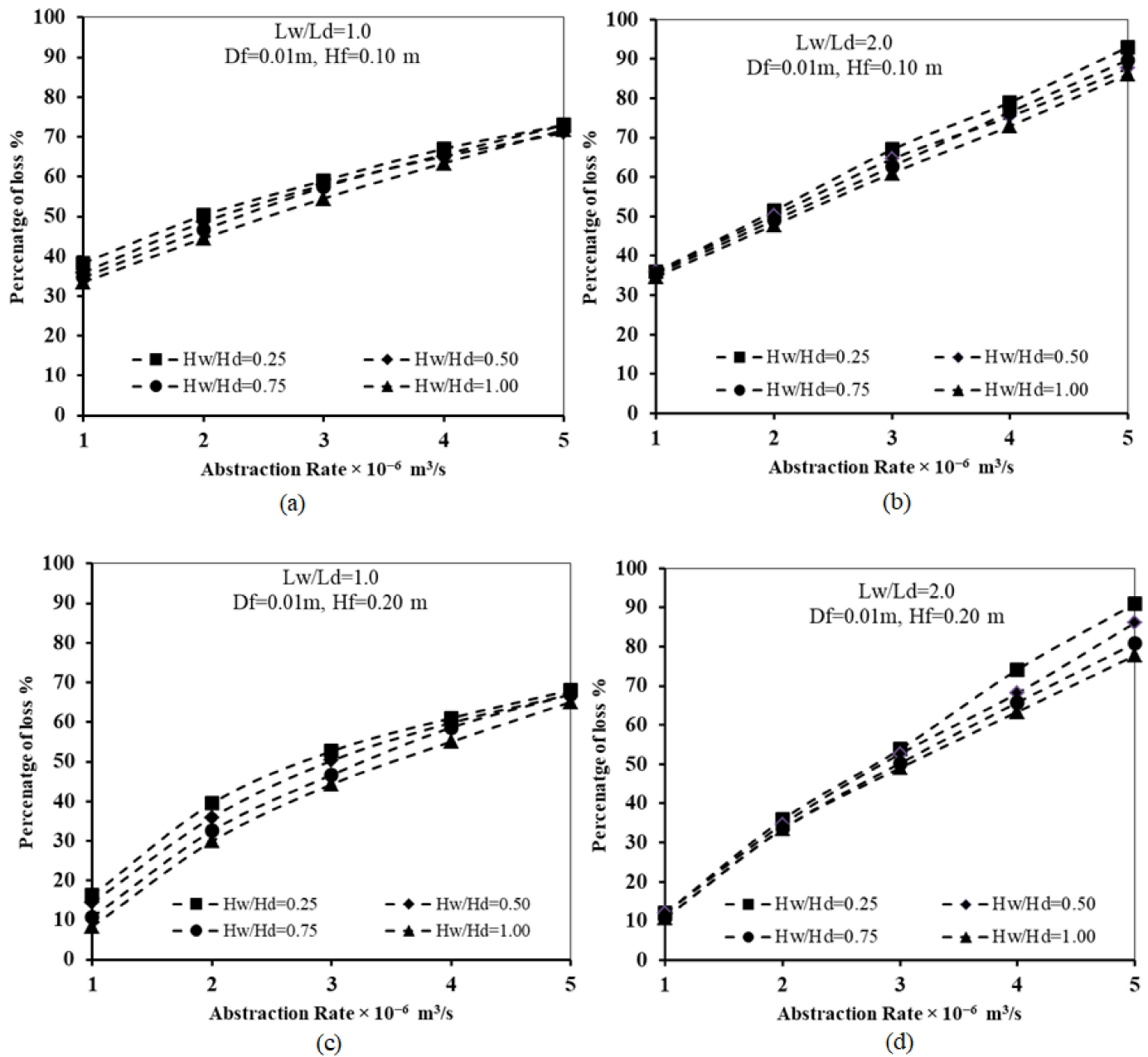


Figure 6. Relation between abstraction well rate and loss of subsurface dam effectiveness for $L_d = 0.50$ m, $D_f = 0.01$ m, and for different L_w/L_d and H_f : (a) $L_w/L_d = 1.0$ and $H_f = 0.1$, (b) $L_w/L_d = 2.0$ and $H_f = 0.1$, (c) $L_w/L_d = 1.0$ and $H_f = 0.2$, and (d) $L_w/L_d = 2.0$ and $H_f = 0.2$.

4.3. Impact of Well Height on the Loss of Effectiveness of Subsurface Dam to Control Seawater Intrusion

All simulated tests to explore the influence of the well location were implemented with $D_f = 0.001$ m, a subsurface dam location $L_d = 50$ cm, for two different values of dimensionless well location ratios L_w/L_d equal to 1.0 and 2.0, and for $H_f = 0.1$ and 0.2 m. The well location was presented by the dimensionless ratio H_w/H_d . Four different values of dimensionless well height ratios were performed: 0.25, 0.50, 0.75, and 1.0.

The results of Figure 7 demonstrated that for various values of the dimensionless well height ratio, increasing the well abstraction rate resulted in an increase in the loss of effectiveness of the subsurface dam. For $L_w/L_d = 1.0$ and $H_f = 0.2$, for $H_w/H_d = 0.25$, the loss of effectiveness increased from 30% to 90% when increasing the rate of abstraction

from 1×10^{-6} to 5×10^{-6} m^3/s , respectively. In addition, for $L_w/L_d = 2.0$ and $H_F = 0.2$, for $H_w/H_d = 0.25$, the loss of effectiveness increased from 28% to 82% when increasing the rate of abstraction from 1×10^{-6} to 5×10^{-6} m^3/s , respectively.

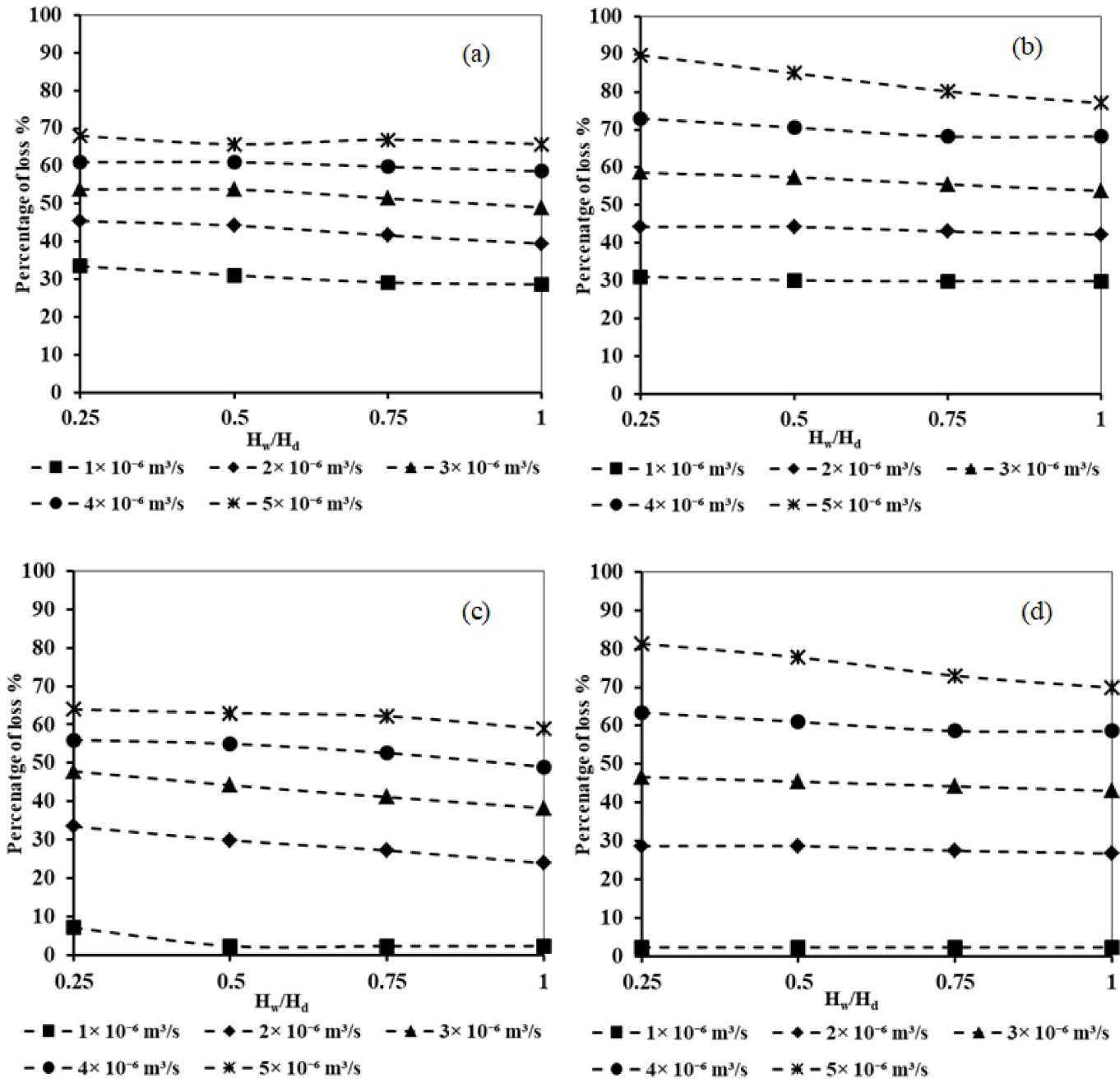


Figure 7. Relation between well height ratio and loss of subsurface dam effectiveness for $L_d = 0.50$ m and $D_f = 0.005$ m for: (a) $L_w/L_d = 1.0$ and $H_F = 0.1$, (b) $L_w/L_d = 2.0$ and $H_F = 0.1$, (c) $L_w/L_d = 1.0$ and $H_F = 0.2$, (d) $L_w/L_d = 2.0$ and $H_F = 0.2$.

Increasing the dimensionless well height ratio from 0.25 to 1.0 resulted in a slight decrease in the loss of effectiveness of the subsurface dam due to fracture and abstraction. For $L_d = 0.5$, $L_w/L_d = 1.0$ and $H_F = 0.2$, the loss of effectiveness decreased from 91% to 77.7% when increasing the well height ratio from 0.25 to 1.0, respectively. In addition, for $L_d = 0.5$, $L_w/L_d = 2.0$ and $H_F = 0.2$, the loss of effectiveness decreased from 81% to 69.8% when increasing the well height ratio from 0.25 to 1.0, respectively. The resulting loss of

effectiveness of the subsurface dam is relatively small for $L_w/L_d = 1.0$ compared with $L_w/L_d = 2.0$ for different well height ratios. The maximum recorded losses of effectiveness were equal to 73 and 68% for an abstraction rate equal to $5 \times 10^{-6} \text{ m}^3/\text{s}$ for H_f values equal to 0.1 and 0.2, respectively.

Comparison of the results in Figure 8 with Figure 7 demonstrated that increasing the fracture aperture from 0.0005 to 0.01 m resulted in an obvious increase in the loss of effectiveness of the subsurface dam. A slight decrease in the loss of effectiveness was observed for different abstraction rates when increasing the well height ratio from 0.25 to 1.0. The percentage of loss decreased slightly from 93% to 86% when increasing the well height ratio from 0.25 to 1.0, respectively. For $L_w/L_d = 2.0$, the maximum recorded percentage of loss equal 93% and 90.9% for H_f equal 0.1 and 0.2, respectively. For $L_w/L_d = 1.0$, the maximum recorded percentage of loss equal 73% and 68% for H_f equal 0.1 and 0.2, respectively. When the dimensionless value of the well height location L_w/L_d is increased from 1.0 to 2.0, the effectiveness of the subsurface dam is reduced by around 20%. It can be noticed from the findings of Figures 7 and 8 that the well height ratio has a slight effect on the loss of subsurface effectiveness. As the height of seawater above the fracture location increased, upstream of the dam, the volume of transported seawater from upstream to downstream through the fracture in the subsurface dam increased. As a result, installing the groundwater well near the bottom of the dam and the aquifer bottom, in case of a fracture height equal 0.1 m, causes more seawater to travel through the opening of the subsurface dam than in the case of a fracture height $H_f = 0.2$ m.

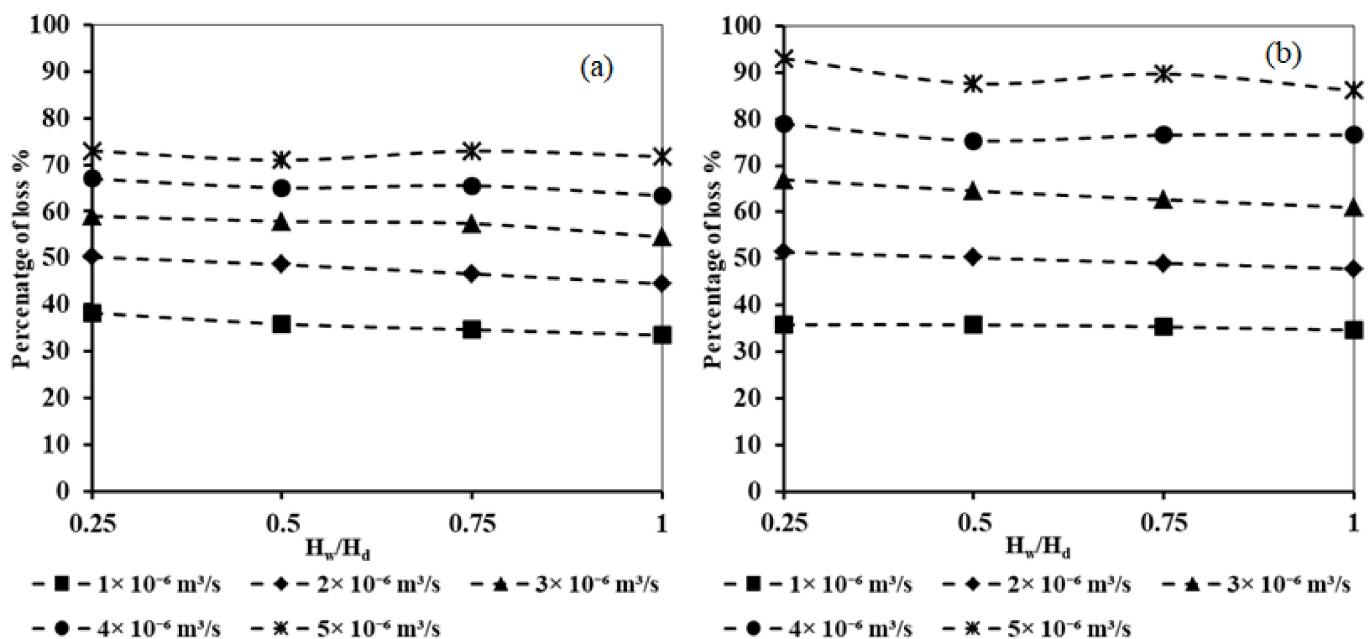


Figure 8. Cont.

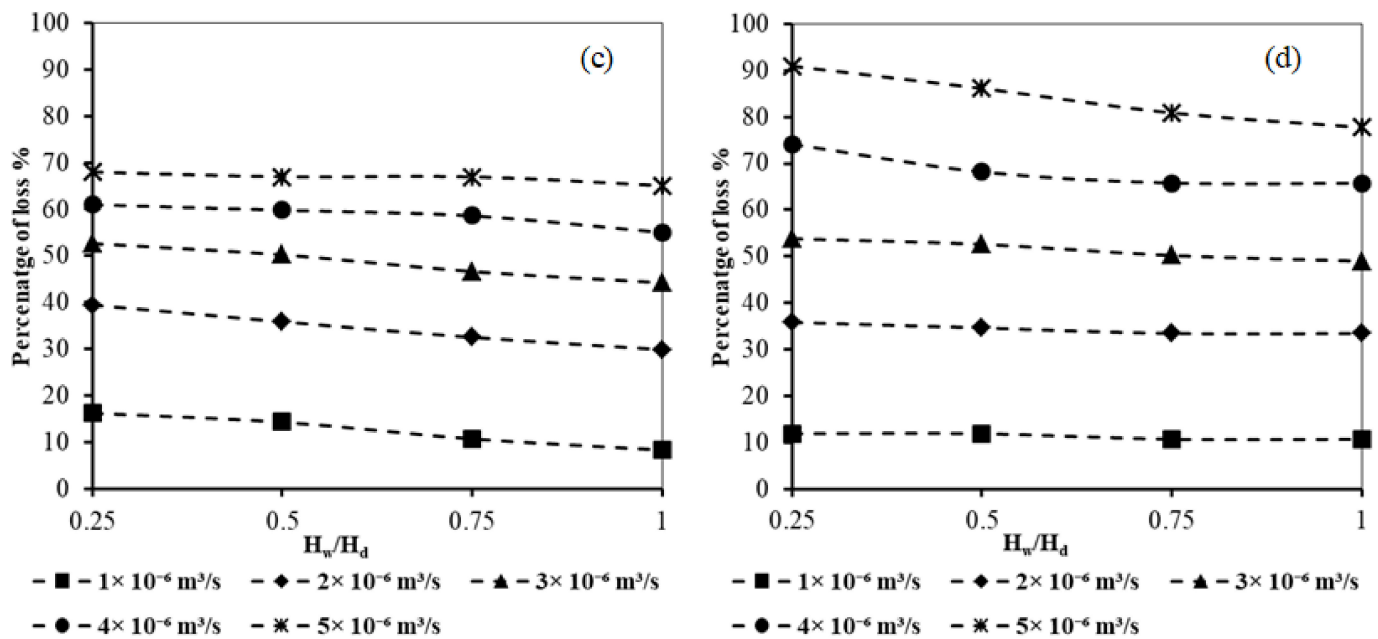


Figure 8. Relation between well height ratio and loss of subsurface dam effectiveness for $L_d = 0.50$ m and $D_f = 0.01$ m for: (a) $L_w/L_d = 1.0$ and $H_f = 0.1$, (b) $L_w/L_d = 2.0$ and $H_f = 0.1$, (c) $L_w/L_d = 1.0$ and $H_f = 0.2$, (d) $L_w/L_d = 2.0$ and $H_f = 0.2$.

4.4. Impact of Well Location on the Loss of Effectiveness of Subsurface Dam to Control Seawater Intrusion

All simulations were run with $L_d = 0.30$ m and $H_f = 0.1$ m for five different abstraction rate values ranging from 1×10^{-6} to 5×10^{-6} m³/s and two different values of D_f and L_w/L_d to see how well location affects the loss of effectiveness of a subsurface dam. As shown in Figure 9, increasing the abstraction rate from 1×10^{-6} to 5×10^{-6} m³/s resulted in an increase in the loss of effectiveness of the subsurface dam for all simulation results and for various values of H_w/H_d varying from 0.25 to 1.0.

Increasing the value of well location L_w/L_d from 1.0 to 2.0 resulted in an increase in subsurface dam’s effectiveness for $L_d = 0.30$ m, $H_f = 0.1$ m, and $D_f = 0.005$ m. The maximum percentages of subsurface dam effectiveness were recorded as 62.2% and 82.12% for L_w/L_d equal to 1.0 and 2.0, respectively, for the abstraction rate of 5×10^{-6} m³/s. In addition, the maximum reductions in the subsurface dam effectiveness reached 75.5% and 88.5% for $L_D = 0.30$ m, $H_f = 0.1$ m, and $D_f = 0.005$ m for L_w/L_d of 1.0 and 2.0, respectively. By relocating the well farther from the subsurface dam, the penetration of seawater intrusion into freshwater was increased, and the loss of the subsurface dam’s effectiveness was increased.

When the values of fracture height H_f were increased from 0.1 to 0.2, the loss of effectiveness of the subsurface dam decreased marginally, as shown in Figures 9 and 10.

For $D_f = 0.005$ m, $L_w/L_d = 1.0$ and 2.0, and an abstraction rate equal to 1×10^{-6} m³/s, the minimum values of the loss of subsurface dam effectiveness are about 38.25% and 39.7%. Increasing the value of L_w/L_d from 1.0 to 2.0 resulted in an increase in the loss of effectiveness of the subsurface dam for $D_f = 0.01$ m, with the minimum recorded values equaling 44.25 and 46.6%, respectively. It can be concluded from the comparison of the results for of Figures 9 and 10 that positioning the groundwater well far away from the underground dam forced large amounts of saltwater to travel through the fracture aperture in the subsurface dam and move downstream of the underground dam until reaching the screen of the groundwater well. As a result, the seawater intrusion’s penetration length increased when installing the groundwater well farther away from the location of the underground dam. In addition, the loss of subsurface dam effectiveness was reduced.

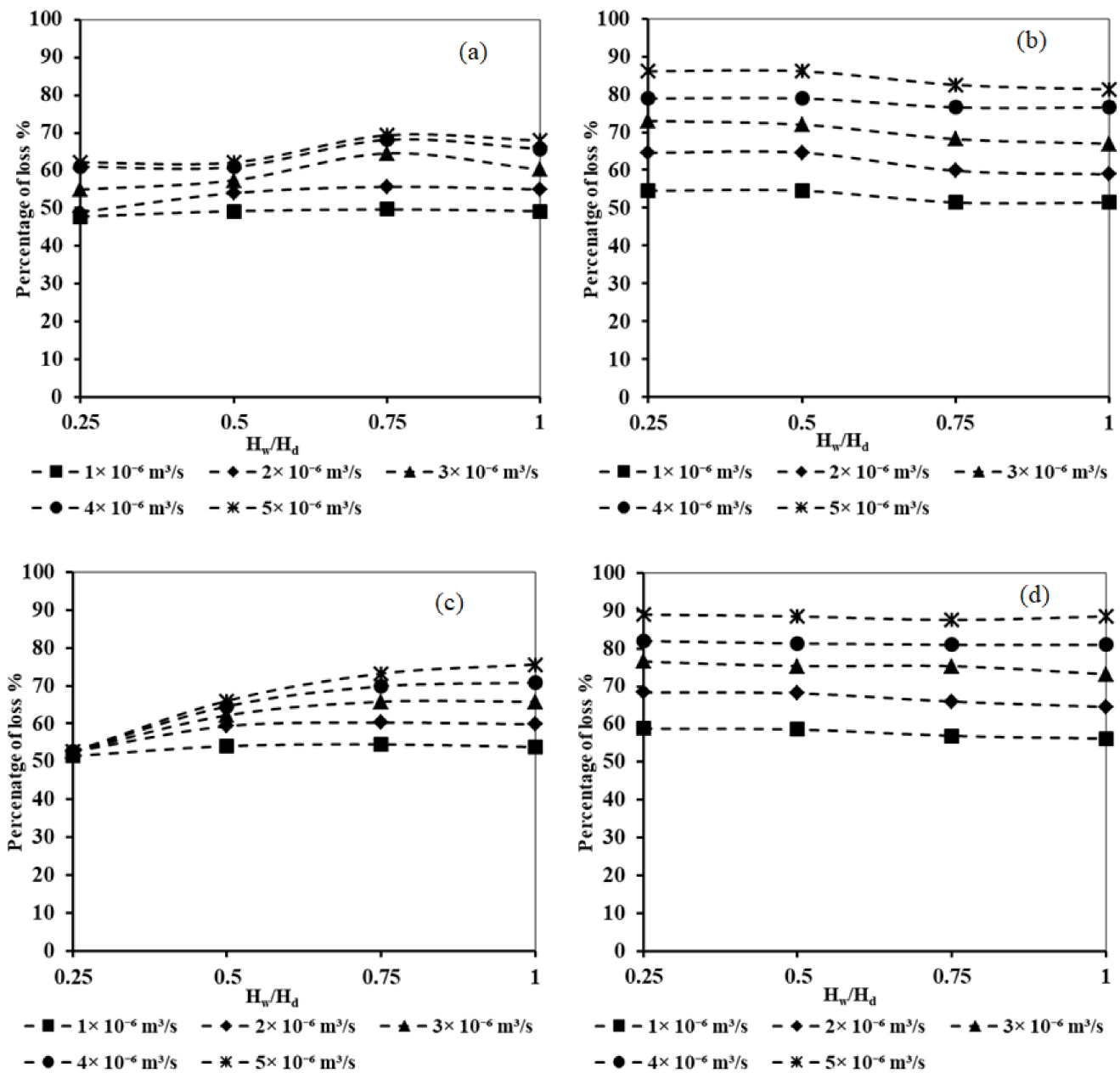


Figure 9. Relation between well location ratio and loss of subsurface dam effectiveness for $L_d = 0.30$ m and $H_f = 0.1$ m for: (a) $L_w/L_d = 1.0$ and $D_f = 0.005$ m, (b) $L_w/L_d = 2.0$ and $D_f = 0.005$ m, (c) $L_w/L_d = 1.0$ and $D_f = 0.01$ m, (d) $L_w/L_d = 2.0$ and $D_f = 0.01$ m.

4.5. Impact of Subsurface Dam Height on the Loss of Effectiveness of Subsurface Dam to Control Seawater Intrusion

All simulated situations to examine the impact of the subsurface dam height were run with a fracture height $H_f = 0.1$ m, $D_f = 0.001$ m, subsurface dam location $L_d = 50$ cm, and a dimensionless well location ratio L_w/L_d equal to 2.0.

As shown in Figure 11, the impact of the subsurface dam height on loss of the subsurface dam’s effectiveness was checked for various values of subsurface dam height, 50, 60, 70, and 80 cm, and for five abstraction rate values varying from 1×10^{-6} to 5×10^{-6} m³/s.

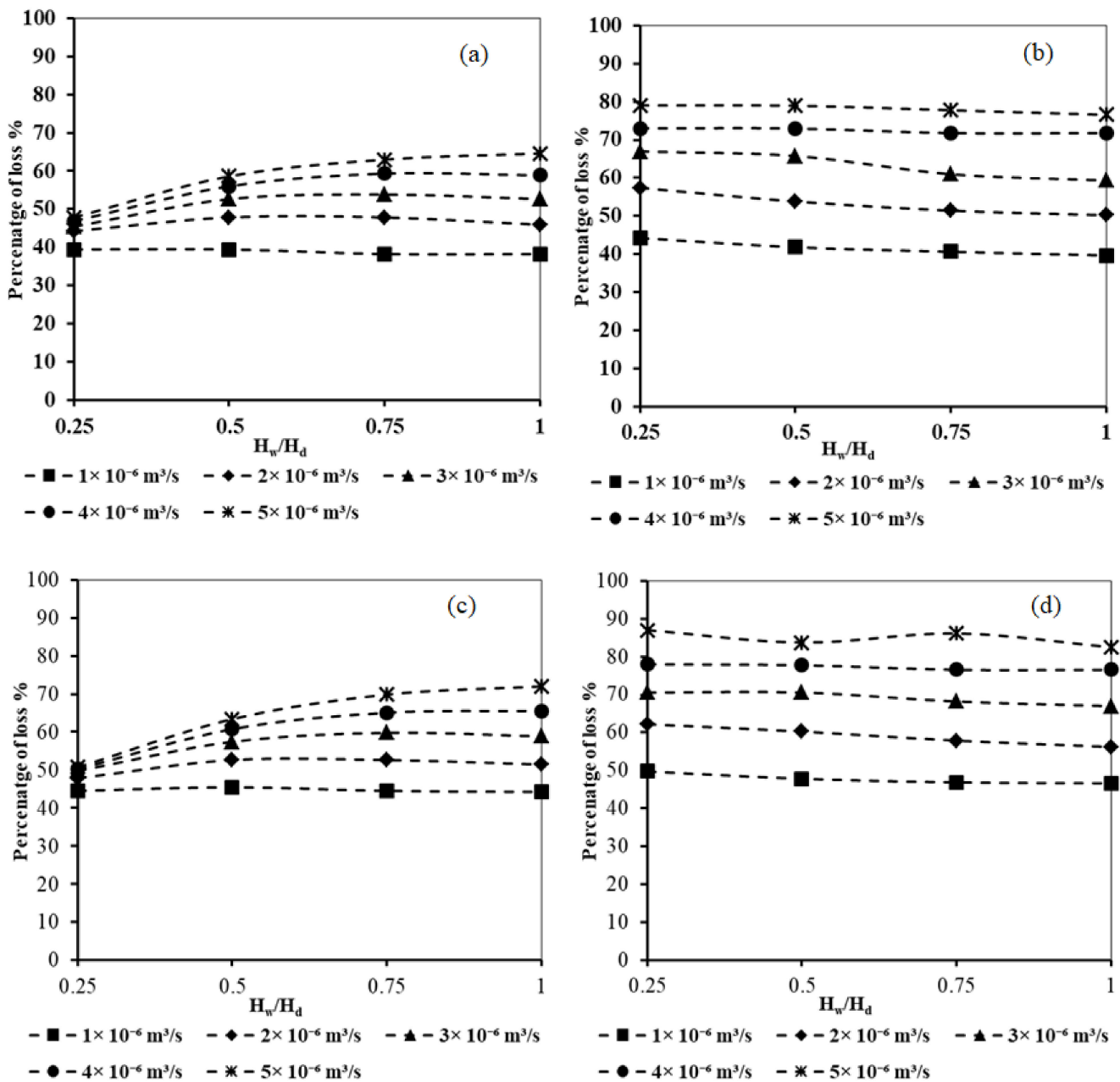


Figure 10. Relation between well location ratio and loss of subsurface dam effectiveness for $L_d = 0.30 \text{ m}$ and $H_f = 0.2 \text{ m}$ for: (a) $L_w/L_d = 1.0$ and $D_F = 0.005 \text{ m}$, (b) $L_w/L_d = 2.0$ and $D_F = 0.005 \text{ m}$, (c) $L_w/L_d = 1.0$ and $D_F = 0.01 \text{ m}$, (d) $L_w/L_d = 2.0$ and $D_F = 0.01 \text{ m}$.

It can be noticed from Figure 11 that the loss of effectiveness of the subsurface dam decreases when increasing the subsurface dam height. Increasing the well abstraction rate caused the loss of effectiveness of the subsurface dam to increase. The percentage of loss of subsurface dam effectiveness decreased dramatically from 32% to 3% when increasing the subsurface dam height from 50 to 80 cm for an abstraction rate equal to $1 \times 10^{-6} \text{ m}^3/\text{s}$. The loss of effectiveness of the subsurface dam decreased slightly when increasing the well height ratio from 0.25 to 1.0. The maximum losses of effectiveness, equal to 91% and 81%, were recorded at subsurface dam heights equal to 50 cm for $H_w/H_d = 0.25$ and 1.0, respectively. The shortest subsurface dam caused the saltwater upstream of the dam to overflow above the top of dam. Moreover, the penetration of seawater increases more with the increase in the abstraction rate, and the loss of effectiveness raised. The results of

Figure 11 demonstrate that the underground dam height has a significant impact on the loss of effectiveness of the subsurface dam. A shorter subsurface dam height caused the saltwater upstream of the dam to overflow above the top of the subsurface dam, and as a result, the area of seawater downstream of the dam increased, the length of the sweater wedge penetration increased, and the loss of effectiveness increased. This result is obvious, mainly in the case of a combination between a shorter dam height and a groundwater well positioned away from the aquifer bottom and near the crest of the underground dam.

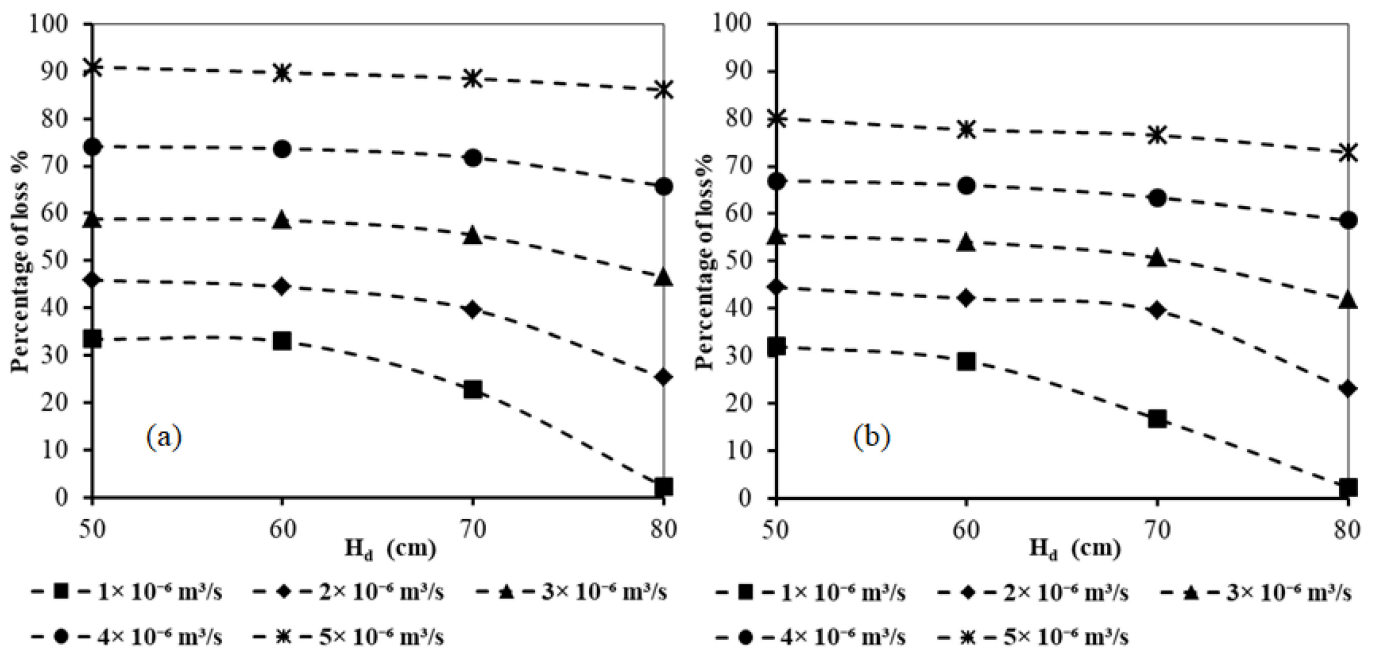


Figure 11. Relation between subsurface dam height and loss of subsurface dam effectiveness for $L_d = 0.50$, $D_F = 0.005$ m, $H_f = 0.1$ m, and $L_w/L_d = 2.0$ for: (a) and $H_w/H_d = 0.25$, and (b) $H_w/H_d = 1.0$.

4.6. Impact of Subsurface Dam Location on the Loss of Effectiveness of Subsurface Dam to Control Seawater Intrusion

All simulations were run with a saltwater density of 1025 kg/m^3 , $D_F = 0.005$ m, and $L_w/L_d = 1.0$ for five different abstraction rates ranging from 1×10^{-6} to $5 \times 10^{-6} \text{ m}^3/s$ to evaluate the influence of subsurface dam location. Two L_d values of 0.30 and 0.50 m were investigated.

As presented in Figure 12, for different values of L_d , the loss of effectiveness of the subsurface dam increases with the increasing abstraction rate. For a subsurface dam with $L_d = 0.5$ m, increasing the well height ratio H_w/H_d from 0.25 to 1.0 causes the loss of effectiveness to decrease for two different values of fracture height, 0.1 and 0.2 m. For an aperture fracture with a height H_f of 0.2, the resulting loss of effectiveness was slightly less compared with $H_f = 0.1$ m.

Decreasing the distance from the seaside to the subsurface dam from 0.50 to 0.30 m resulted in increasing the loss of effectiveness of the subsurface dam. In addition, the percentage of loss increased with the increase in the well height from the bottom of the aquifer. The maximum loss reduction was observed for $H_f = 0.1$ and 0.2 m to be about 68% and 64.5%, respectively.

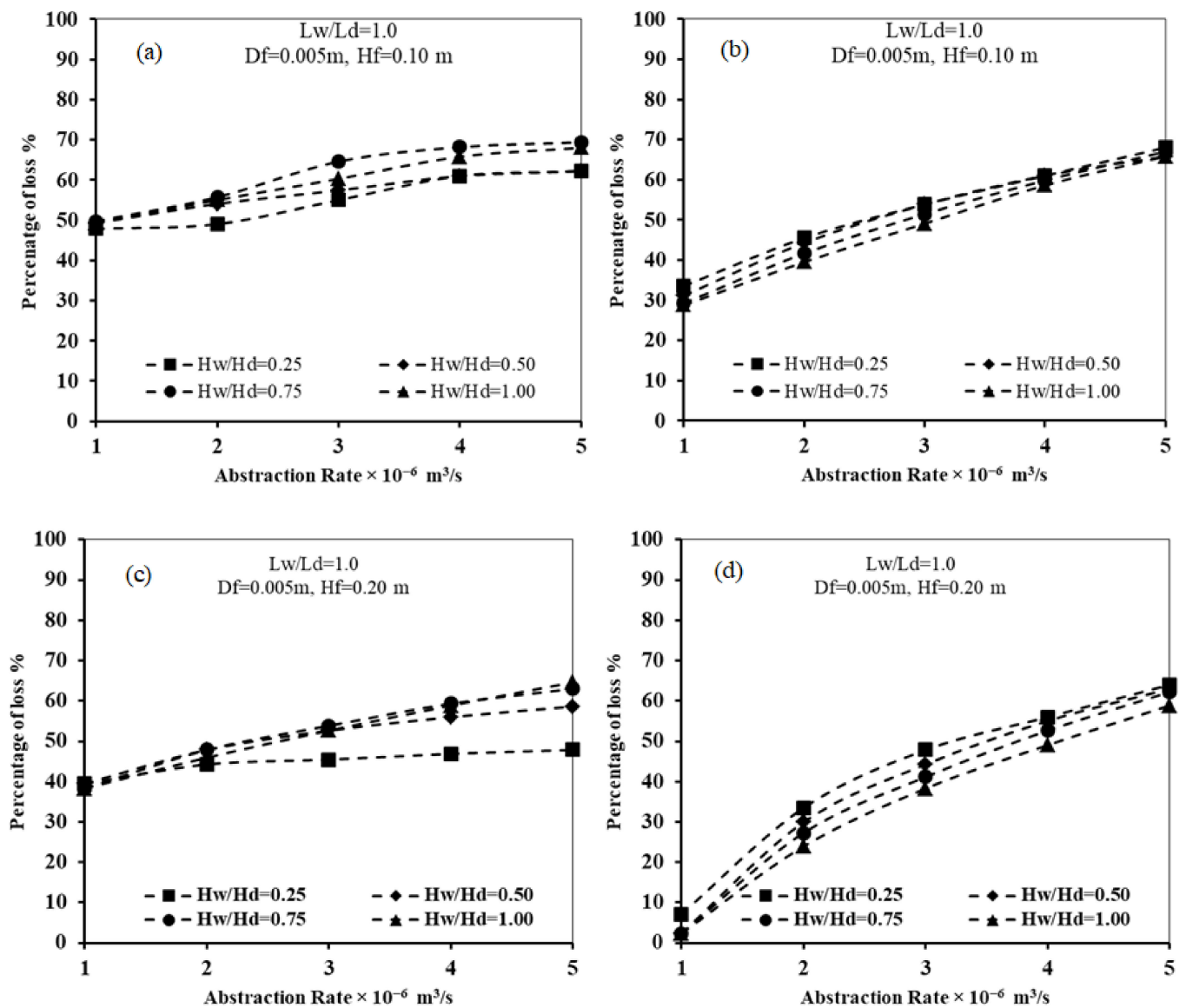


Figure 12. Relation between abstraction rate and loss of subsurface dam effectiveness for $D_f = 0.005$ m and $L_w/L_d = 1.0$ for different values of subsurface dam location: (a) $L_d = 0.30$, $H_f = 0.1$ m (b) $L_d = 0.50$, $H_f = 0.1$ m (c) $L_d = 0.30$, $H_f = 0.2$ m, and (d) $L_d = 0.50$, $H_f = 0.2$ m.

Figure 13 presents the loss of effectiveness of a subsurface dam for different abstraction rates ranging from 1×10^{-6} to 5×10^{-6} m^3/s , for $L_w/L_d = 1.0$, and for $D_f = 0.01$ m for two different values of $H_f = 0.1$ and 0.2 m. For $L_d = 0.3$ m, the maximum loss of reduction was recorded for $H_f = 0.1$ and 0.2 m to be about 75.5% and 82.5%, respectively. In addition, for $L_d = 0.5$ m, the maximum loss of reduction in the cutoff wall effectiveness was recorded to be about 71.8% and 67% for $H_f = 0.1$ and 0.2 m, respectively. Increasing the diameter of the fracture aperture in the underground dam leads to an increase in the amount of saltwater that passes through the opening from the dam body. This is because the fracture discharge passing through the fracture aperture increases with the increase in the area of the opening. As a result of that, the fracture discharge increased with the increase in D_f from 0.005 m to 0.01 m, a sequence in which the performance of the subsurface dam decreased. Comparing the results of Figures 11 and 12 confirmed that increasing the diameter of the fracture aperture from $D_f = 0.005$ to 0.1 m caused more seawater to pass through the fracture. The penetration of seawater also increased as the loss of subsurface dam effectiveness increased.

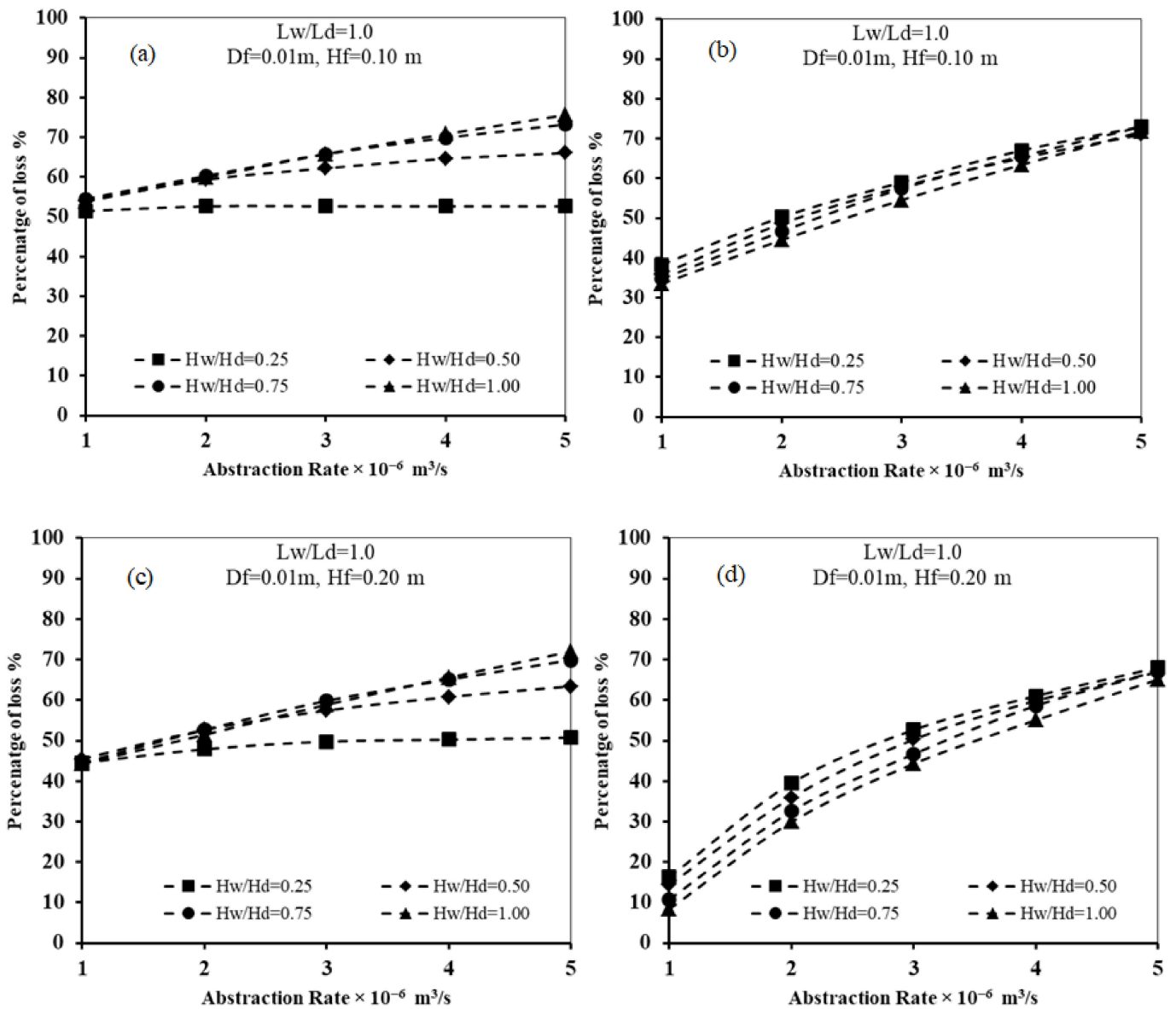


Figure 13. Relation between abstraction rate and loss of subsurface dam effectiveness $D_f = 0.01\text{ m}$ and $L_w/L_d = 1.0$ for different values of subsurface dam location: (a) $L_d = 0.30\text{ m}$, $H_f = 0.1\text{ m}$ (b) $L_d = 0.50\text{ m}$, $H_f = 0.1\text{ m}$ (c) $L_d = 0.30\text{ m}$, $H_f = 0.2\text{ m}$, and (d) $L_d = 0.50\text{ m}$, $H_f = 0.2\text{ m}$.

4.7. Impact of Saltwater Density on the Loss of Effectiveness of Subsurface Dam to Control Seawater Intrusion

All simulated situations to explore the influence of the seawater density were run with fracture height $H_f = 0.1\text{ m}$, $D_f = 0.01\text{ m}$, subsurface dam height $H_d = 60\text{ cm}$, dam location $L_d = 0.50\text{ m}$, and a dimensionless well location ratio L_w/L_d equal to 2.0.

As shown in Figure 14, the impact of saltwater density on the percentage of loss of subsurface dam effectiveness was investigated for different values of saltwater density varying between 1022 kg/m^3 and 1030 kg/m^3 for well height ratios H_w/H_d equal to 0.25 and 1.0.

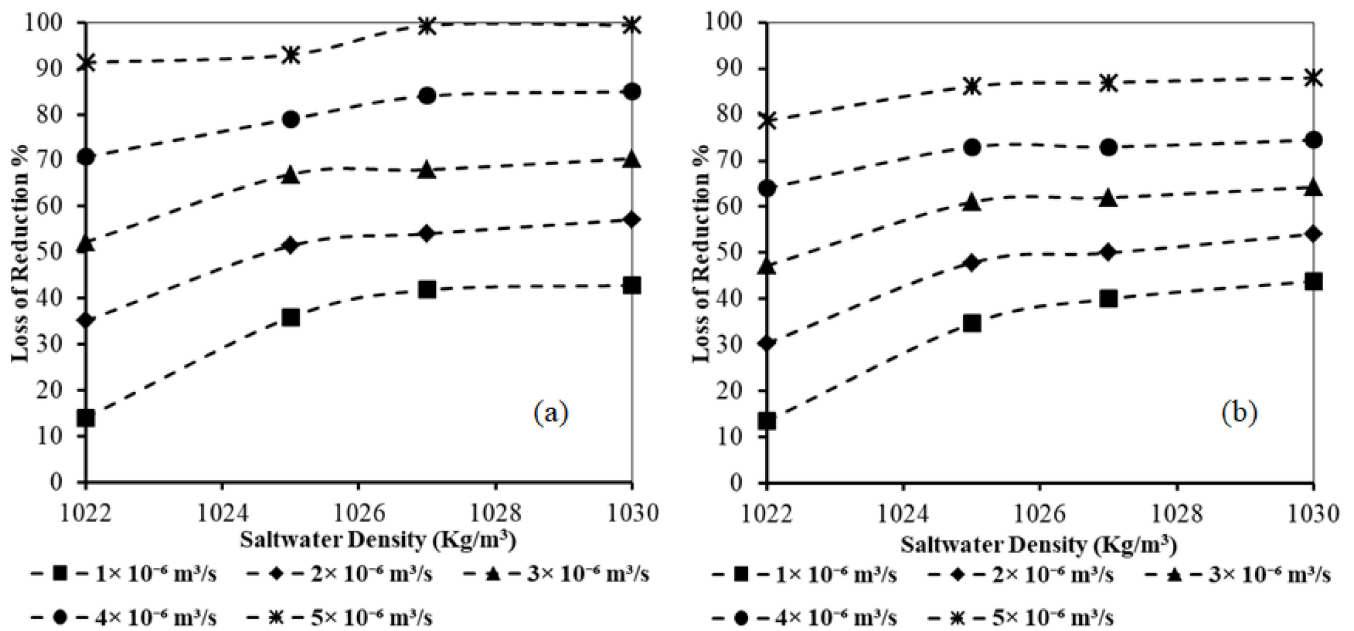


Figure 14. Relation between saltwater density and loss of subsurface dam effectiveness $D_F = 0.01$ m, $H_f = 0.1$ m, and $L_w/L_d = 2.0$ for different values of H_w/H_d : (a) 0.25, (b) 1.0.

With increased saltwater density, the subsurface dam’s effectiveness deteriorates as the loss of the subsurface dam’s effectiveness increases. The loss of the subsurface dam effectiveness rises when raising the extraction rate from the well. The lowest loss was found at a saltwater density equal to 1022 kg/m³, which is roughly 13 percent with an abstraction rate equal to 1 × 10⁻⁶ m³/s. The maximum loss was reported at a saltwater density equal to 1033 kg/m³ and is approximately 99% with an abstraction rate of 5 × 10⁻⁶ m³/s. As a result of the simulation’s findings, we can deduce that high seawater density causes a high-density drive, allowing more saltwater to penetrate the freshwater side. In addition, the penetration of the saltwater advances more when increasing the abstraction rate. Moving the well from $H_w/H_d = 0.25$ to 1.0 far away from the bottom of the subsurface dam results in a slight decrease in the loss of subsurface dam effectiveness. The maximum loss was reported at a saltwater density equal to 1033 kg/m³ and is approximately 86% with an abstraction rate of 5 × 10⁻⁶ m³/s for H_w/H_d equals 1.0.

Figure 15 displays the comparison between the losses of subsurface dam effectiveness for two different values of saltwater density, 1025 and 1030 kg/m³, for $L_w/L_d = 2.0$, $D_F = 0.01$ m, $H_f = 0.1$ m, and well height ratios of $H_w/H_d = 0.25, 0.50, 0.75,$ and 1.0. When the abstraction rate from a groundwater well is increased, the loss of effectiveness of the subsurface dam increases. Increasing the well height ratio H_w/H_d from 0.25 to 1.0 results in increasing the loss of effectiveness from 33% to 40%, respectively, for an abstraction rate equal to 1 × 10⁻⁶ m³/s and from 86% to 89%, respectively, for an abstraction rate equal to 5 × 10⁻⁶ m³/s. Increasing the seawater density from 1025 kg/m³ to 1030 kg/m³ causes the seawater to advance more, and the loss of effectiveness increased from 92% to 94% for an abstraction rate equal to 5 × 10⁻⁶ m³/s. Increasing the seawater density from 1025 kg/m³ to 1030 kg/m³ causes the seawater to advance more, and the loss of effectiveness increased from 34% to 43% for an abstraction rate equal to 1 × 10⁻⁶ m³/s.

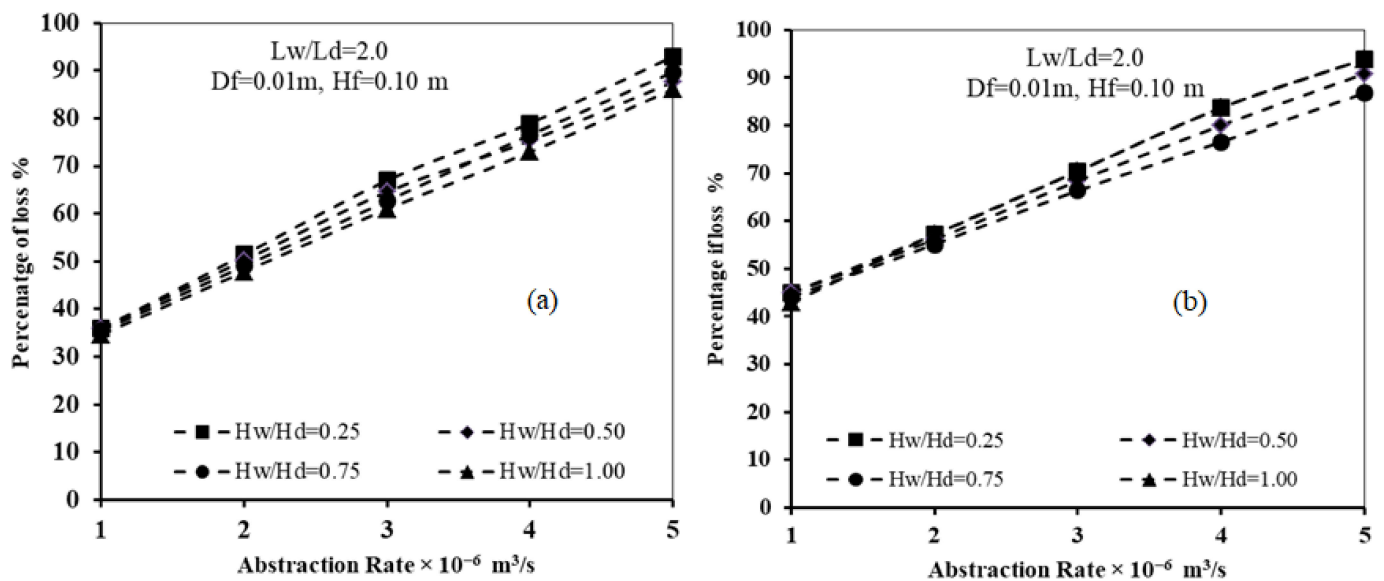


Figure 15. Relation between abstraction rate and loss of subsurface dam effectiveness $D_F = 0.01\text{ m}$, $H_f = 0.1\text{ m}$ for different values of saltwater density: (a) density = 1025 kg/m^3 (b) density = 1030 kg/m^3 .

Comparing the results of Figures 14 and 15 confirmed that increasing the seawater density of the coastal boundary has a significant impact on reducing the effectiveness of the subsurface dam in preventing and controlling seawater intrusion. Increasing the density of seawater from 1025 to 1030 kg/m^3 forced a large amount of seawater to travel through the fracture opening from the upstream side of the dam to the downstream side. The main reason for this is that the seawater head above the fracture opening is mainly dependent on the height of the seawater above the fracture opening and the density of the seawater upstream of the dam. A large volume of seawater moved through the opening in the case of high seawater density and lower fracture aperture height in the underground dam. In addition, increasing the abstraction rate of the groundwater well caused the seawater to travel downstream of the underground dam through the fracture opening and finally reach the screen of the groundwater well.

The repulsion ratio of seawater intrusion wedge increased when positioning the underground dam closer to the seawater side. This finding is compatible with the previous published research of Luyun et al. [12], Anwar [11], and Armanuos et al. [13]. The achieved repulsion ratios were equal to 40.47% and 64.38% for subsurface dams located at distances $L_d = 0.50\text{ m}$ and 0.3 m , respectively. The results confirmed that installing the groundwater well downstream of the underground dam has a significant impact on increasing the seawater wedge length and minimizing the effectiveness of the submerged dam to control seawater intrusion. Comparing the results of the current study with Laabidi et al. [19] confirmed that the loss of effectiveness increased to reach 66.98%, 74.16%, and 81.33% for cases of abstraction rates equal to 3×10^{-6} , 4×10^{-6} , and $5 \times 10^{-6}\text{ m}^3/\text{s}$, respectively, where the achieved repulsion ratio without fracture equals 64.11%. These results were presented as an example for $H_d = 0.6\text{ m}$, $D_f = 0.005\text{ m}$, $H_f = 0.1\text{ m}$, $L_w/L_d = 2.0$, and $H_w/H_d = 0.25$. The loss of subsurface dam effectiveness increased when increasing the diameter of the fracture from $D_f = 0.005\text{ m}$ to 0.01 m ; this agrees with the results of Laabidi et al. [19] for horizontal fractures. Finally, the achieved loss of effectiveness of the subsurface dam after installing the abstraction well is higher than the fracture only case in the underground dam (Laabidi et al. [19]).

4.8. Distribution of Seawater Intrusion for Different Presented Simulation Scenarios

The following sections present the seawater distributions for various selected scenarios of fracture aperture, fracture height, subsurface dam location, groundwater well location, subsurface dam height, and seawater density. These were presented for different abstraction well rates ranging from 2×10^{-6} to 5×10^{-6} m³/s.

4.9. Distribution of Seawater Intrusion for Different Fracture Aperture and Fracture Height Scenarios

Figure 16 depicts the salinity distribution for $D_F = 0.005$ m, $L_d = 0.5$ m, $H_w/H_d = 0.25$, $H_d = 60$ cm, for five different values of abstraction rates: are 2×10^{-6} , 3×10^{-6} , 4×10^{-6} , and 5×10^{-6} m³/s for fracture height $H_f = 0.1$. The penetration length of seawater was 78, 88, 95, 98, and 101 cm measured from the seaside boundary and equaled 56, 78, 90, 96, and 99 cm for fracture heights $H_f = 0.1$ and 0.2 m, respectively. Increasing the H_f from 0.1 to 0.2 resulted in decreasing the penetration length of seawater intrusion. The maximum loss of effectiveness of the subsurface dam decreased from 61.00 to 58.61% when increasing the fracture height from 0.10 to 0.20 m, respectively, for an abstraction rate equal to 5×10^{-6} m³/s. The minimum loss of effectiveness of the subsurface dam decreased from 33.49 to 7.17% when increasing the fracture height from 0.10 to 0.20 m, respectively, for an abstraction rate equal to 1×10^{-6} m³/s.

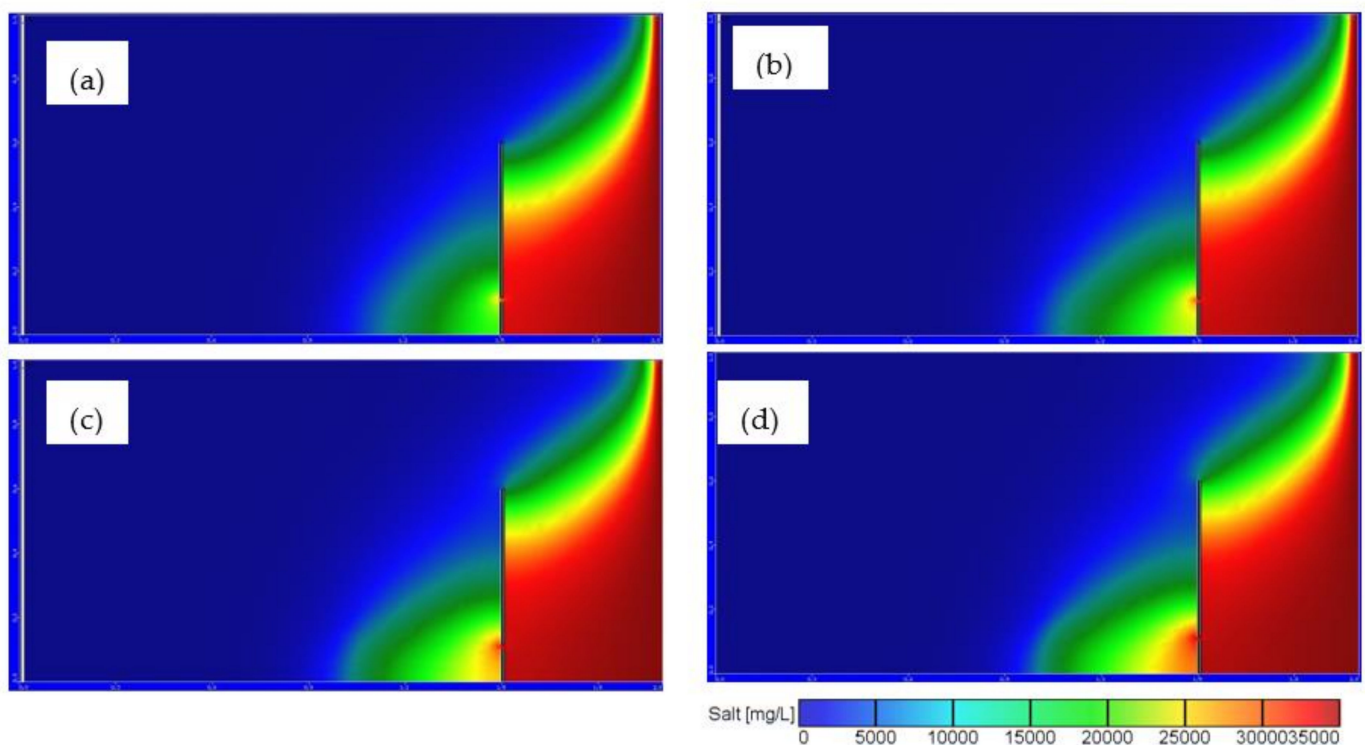


Figure 16. Salinity distribution for $D_F = 0.005$ m, $L_d = 0.5$ m, $H_w/H_d = 0.25$ for fracture height $H_f = 0.1$ m and for different values of abstraction rates: (a) 2×10^{-6} (b) 3×10^{-6} , (c) 4×10^{-6} , and (d) 5×10^{-6} m³/s.

Figure 17 shows the salinity distribution for $D_F = 0.01$ m, $L_d = 0.5$ m, $H_w/H_d = 0.25$, and $H_d = 60$ cm for five different abstraction rates of 2×10^{-6} , 3×10^{-6} , 4×10^{-6} , and 5×10^{-6} m³/s and for a fracture height $H_f = 0.1$. The losses of effectiveness of the subsurface dam were 38.27, 50.23, 57.41, 61.04, and 63.39% (for fracture height $H_f = 0.10$ m) and equaled 16.26, 39.47, 52.63, 58.61, and 61.72% (for fracture height $H_f = 0.2$ m) for abstraction rates equal to 1×10^{-6} , 2×10^{-6} , 3×10^{-6} , 4×10^{-6} , and 5×10^{-6} m³/s, respectively. Increasing the H_f from 0.1 to 0.2 resulted in decreasing in the penetration

length of seawater intrusion. The maximum length of the seawater intrusion wedge decreased from 103 to 101.6 cm measured from the seaside when increasing the fracture height from 0.10 to 0.20 m, respectively, for an abstraction rate equal to $5 \times 10^{-6} \text{ m}^3/\text{s}$. The minimum penetration length of the seawater wedge decreased from 82 to 63.60 cm when increasing the fracture height from 0.10 to 0.20 m, respectively, for an abstraction rate equal to $1 \times 10^{-6} \text{ m}^3/\text{s}$.

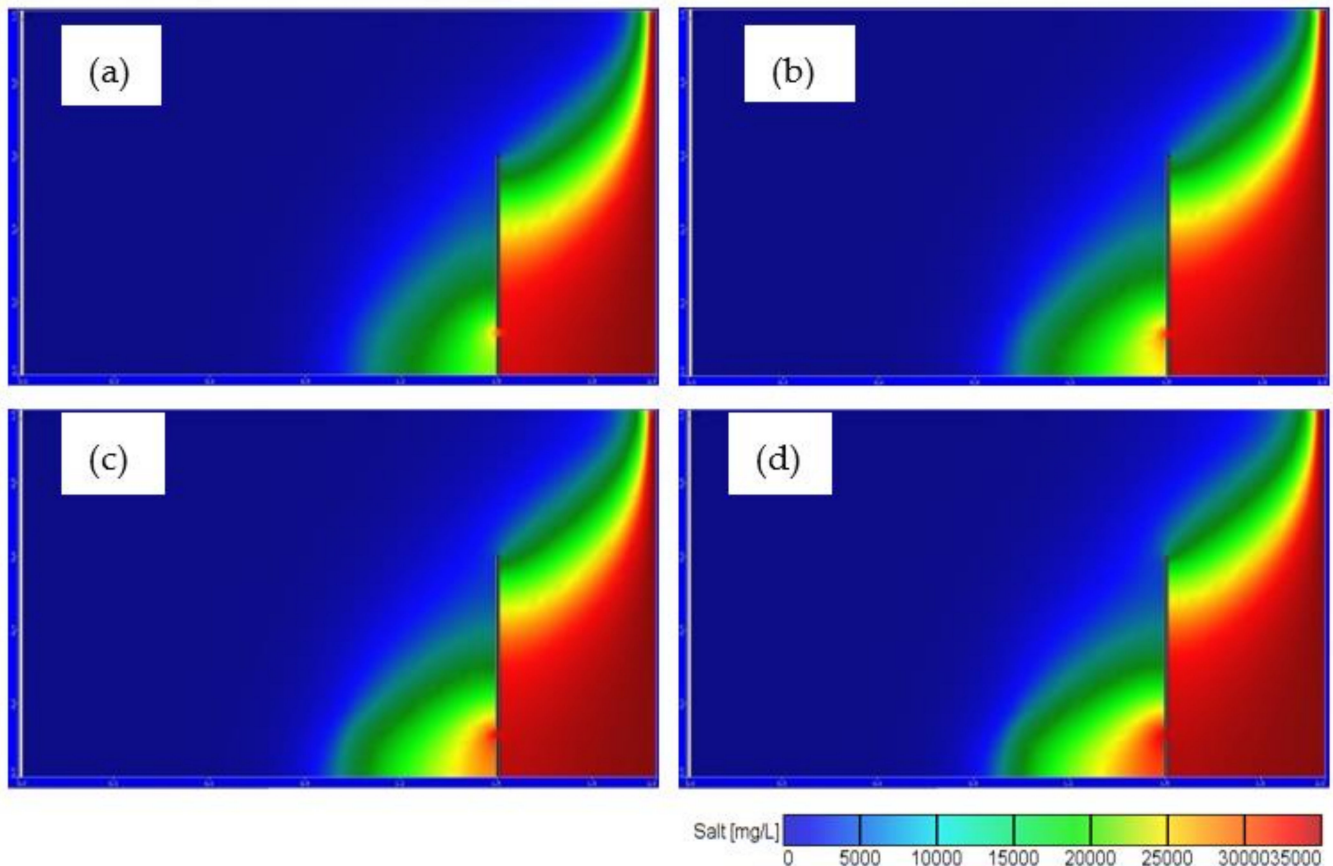


Figure 17. Salinity distribution for $D_f = 0.01 \text{ m}$, $L_d = 0.5 \text{ m}$, $H_w/H_d = 0.25$ for fracture height $H_f = 0.1 \text{ m}$ and for different values of abstraction rates: (a) 2×10^{-6} (b) 3×10^{-6} , (c) 4×10^{-6} , and (d) $5 \times 10^{-6} \text{ m}^3/\text{s}$.

Comparing the findings of results of Figure 16 (for $D_f = 0.005 \text{ m}$) with Figure 17 (for $D_f = 0.01 \text{ m}$) confirmed that increasing the diameter of the fracture aperture resulted in an increase in the penetration length of the seawater intrusion wedge, and the loss of effectiveness of subsurface dam increased. For $H_f = 0.10 \text{ m}$, the maximum loss of the underground dam's effectiveness increased from 61.00% to 63.39% for the same abstraction rate of $5 \times 10^{-6} \text{ m}^3/\text{s}$ for $D_f = 0.005 \text{ m}$ and $D_f = 0.01 \text{ m}$, respectively. For $H_f = 0.20 \text{ m}$, the maximum loss of the underground dam's effectiveness increased from 58.61% to 61.72% for the same abstraction rate of $5 \times 10^{-6} \text{ m}^3/\text{s}$ for $D_f = 0.005 \text{ m}$ and $D_f = 0.01 \text{ m}$, respectively.

4.10. Distribution of Seawater Intrusion for Different Well Location Scenarios

Figure 18 shows the transient seawater intrusion for $D_f = 0.005 \text{ m}$, $H_f = 0.1 \text{ m}$, $L_d = 0.5 \text{ m}$, $H_w/H_d = 0.25$, and $Q_w = 5 \times 10^{-6} \text{ m}^3/\text{s}$ for a well location ratio $L_w/L_d = 1.0$ at five different transient times of 5, 25, 50, 75, and 100 min and for two different values of well location ratio $L_w/L_d = 1.0$. The penetration length of the seawater wedge increased when increasing the time; the length reached 86, 92, 112, 124, and 136 cm measured from the sea boundary (for $L_w/L_d = 2.0$) and reached 68, 100, 108, 112, and 114 cm measured from the seaside (for $L_w/L_d = 1.0$). The seawater wedge reached the steady state condition at time equal 100 min

from the beginning of the abstraction. Moving the groundwater well far away from the underground dam caused more seawater to be transported and increased the penetration length of the seawater; consequently, the loss of reduction increased. For an abstraction rate $Q_w = 1 \times 10^{-6} \text{ m}^3/\text{s}$, the maximum loss of effectiveness increased from 76.56% to 98% for $L_w/L_d = 1.0$ and 2.0, respectively.

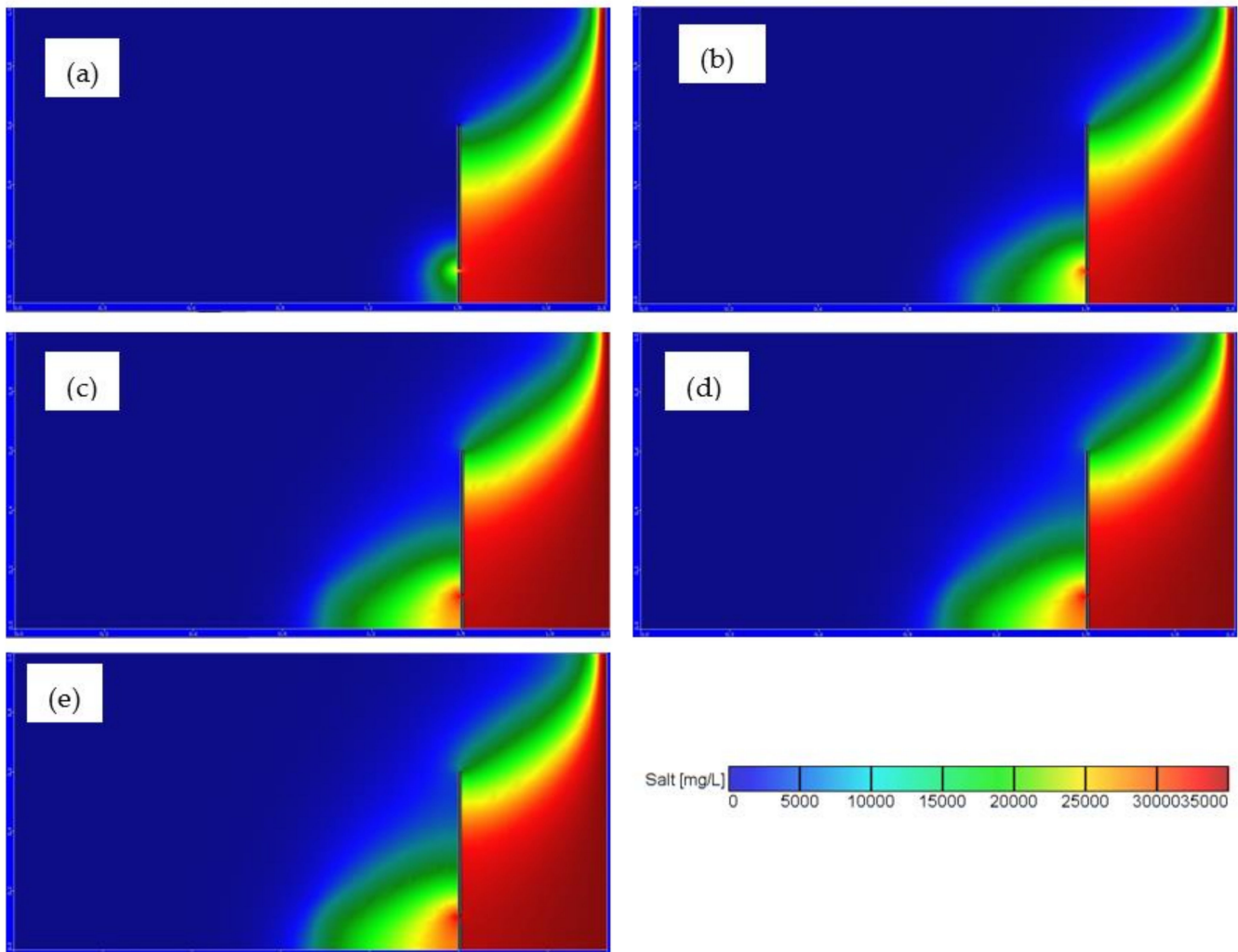


Figure 18. Transient seawater intrusion for $D_f = 0.005 \text{ m}$, $H_f = 0.1 \text{ m}$, $L_d = 0.5 \text{ m}$, $H_w/H_d = 0.25$, $Q_w = 5 \times 10^{-6} \text{ m}^3/\text{s}$ for well location ratio $L_w/L_d = 1.0$ at time transient time: (a) 5 (b) 25, (c) 50, (d) 75, and (e) 100 min.

4.11. Distribution of Seawater Intrusion for Different Subsurface Dam Location Scenarios

Figure A1 describes the salinity distribution for $D_f = 0.005 \text{ m}$, $H_f = 0.1 \text{ m}$, $L_d = 0.5 \text{ m}$, and $L_w/L_d = 1.0$ for different abstraction rates of 2×10^{-6} , 3×10^{-6} , 4×10^{-6} , and $5 \times 10^{-6} \text{ m}^3/\text{s}$ and for two different values of subsurface dam location $L_d = 30 \text{ cm}$ and 50 cm . The penetration length of the seawater wedge increased with the increasing abstraction rate of the groundwater well. Increasing the distance from the seaside to the underground dam resulted in an increase in the percentage of loss of the subsurface dam's effectiveness. The length reached 71.2, 75.2, 78, 81, and 82 cm for different abstraction rates of 1×10^{-6} , 2×10^{-6} , 3×10^{-6} , 4×10^{-6} , and $5 \times 10^{-6} \text{ m}^3/\text{s}$, respectively (for $L_d = 30 \text{ cm}$), and reached 76, 87, 95, 101, and 105 cm, respectively, for $L_d = 50 \text{ cm}$. The minimum percentage of loss of the subsurface dam's effectiveness reduced from 49.28% to 31.00% when increasing the L_d from 30 to 50 cm.

4.12. Distribution of Seawater Intrusion for Different Subsurface Dam Height Scenarios

Figure A2 shows the salinity distribution for $D_F = 0.01$ m, $H_f = 0.1$ m, $L_d = 0.5$ m, and an abstraction rate $Q_w = 5 \times 10^{-6}$ m³/s for four different values of subsurface dam height: 50 cm, 60 cm, 70 cm, and 80 cm. Increasing the height of the subsurface dam caused minimized the penetration length of the seawater wedge behind the dam, and the percentage loss of effectiveness of the subsurface dam reduced. The saltwater penetration length reached 126, 125, 124, and 122 cm for underground dam heights of 50, 60, 70, and 80 cm, respectively, and the corresponding percentages of loss of effectiveness equal 90.91, 89.71, 88.51, and 86.12%, respectively. Increasing the height of the subsurface dam caused the seawater to accumulate upstream of the dam, and only the seawater passes through the fracture opening. On the other hand, the shorter height of the subsurface dam caused the seawater to overflow above the top of the subsurface dam. As a result, the length of seawater length increased, and the percentage loss of effectiveness increased.

4.13. Distribution of Seawater Intrusion for Different Seawater Density Scenarios

Figure A3 presents the salinity distribution for $D_F = 0.01$ m, $H_f = 0.1$ m, and $L_d = 0.5$ m for four different values of saltwater density of 1025 kg/m³, 1025 kg/m³, 1027 kg/m³, and 1030 kg/m³. The results of Figure A3 confirm that increasing the density of the saltwater boundary results in an increase in the penetration length of the seawater wedge and forced a large volume of saltwater to travel through the fracture opening on the subsurface dam. In addition, the concentration of seawater upstream and downstream of the subsurface dam increased. The percentage of loss of effectiveness of the subsurface dam reached 91.92, 93.00, 99.30, and 99.40% for seawater densities equal to 1022, 1025, 1027, and 1030 kg/m³, respectively. Because of that, the fracture discharge depends on the head above the level of the fracture and the fracture opening.

5. Conclusions

The findings of the current research show that groundwater abstraction significantly reduces the effectiveness of fractured subsurface dams in preventing seawater intrusion. Based on the developed SEAWAT code, the sensitivity of different variables' effects on the penetration length of saltwater intrusion was evaluated. The variables were well height and location, underground dam height and location, extraction rate from groundwater well, fracture aperture, and the seawater density. The results confirmed that increasing the pumping discharge from the well resulted in a considerable increase in the penetration of the seawater intrusion wedge, and as a result, the effectiveness of the subsurface dam in controlling seawater intrusion reduced. For well abstraction rates equal to 1×10^{-6} and 5×10^{-6} m³/s, the minimum and highest values of the loss of subsurface dam effectiveness were reported to be 34.6% and 93%, respectively. For an abstraction rate of 5×10^{-6} m³/s, increasing the seawater density from 1025 kg/m³ to 1030 kg/m³ led the seawater to penetrate more, and the loss of effectiveness increased from 92% to 94%. The value of the loss of effectiveness of the subsurface dam increased as the distance from the shoreline to the subsurface dam was reduced from 0.50 to 0.30 m. In addition, as the well was raised above the aquifer's bottom, the proportion of loss grew. For $H_f = 0.1$ and 0.2 m, the highest reduction in subsurface dam effectiveness was found to be around 68% and 64.5%, respectively.

The penetration of saltwater intrusion into freshwater was raised by locating the well far from the subsurface dam, and the loss of the subsurface dam's effectiveness was raised. The effectiveness of the subsurface dam is reduced by roughly 20% when the dimensionless value of well height location L_w/L_d is increased from 1.0 to 2.0.

When the diameter of the fracture hole was increased from $D_f = 0.005$ to 0.1 m, more seawater was allowed to pass through, and the penetration of seawater increased, as did the loss of subsurface dam effectiveness. With an increase in the groundwater abstraction rate, the volume of seawater transported behind the dam from the opening of a fracture in the submerged dam increased. The volume of the transferred seawater via the fracture rose

as the height of seawater above the fracture point increased upstream of the dam. Because the groundwater well was placed close to the dam and the aquifer's bottom, a substantial amount of seawater was able to pass through the fracture opening. The amount of seawater that passes through the aperture opening from the underground dam body increases as the diameter of the fracture aperture is increased. The fracture discharge through a fractured underground dam rises in proportion to the size of the opening. For different height ratios of the groundwater well and various abstraction rates, increasing the fracture diameter resulted in an increase in the loss of subsurface dam effectiveness. For $L_w/L_d = 1.0$, the maximum loss of effectiveness increased from 65% to 73% when increasing the fracture diameter from 0.005 to 0.01 m; in addition, for $L_w/L_d = 2.0$, the maximum values increased from 80% to 90%, whereas the fracture aperture increased from 0.005 to 0.01 m.

Because the groundwater well was placed far away from the underground dam, a huge amount of saltwater was forced to travel through the fracture and downstream of the dam until it reached the groundwater well's screen. A shorter subsurface dam height caused saltwater to travel above the top of the dam, resulting in an increase in the area of seawater downstream of the dam, in the length of the seawater wedge penetration, and in the loss of effectiveness. The height of seawater above the level of the fracture opening and the density of saltwater upstream of the dam determine the seawater head above the level of the fracture opening. The increased density of saltwater forced a considerable amount of seawater to flow through the fracture opening. The anisotropy and heterogeneity of the aquifer are not taken into account in Henry's problem. As a result, the actual arrangement should be examined for future research. The findings of this research can be used for groundwater resource management and protection in coastal aquifers.

Author Contributions: Conceptualization, A.M.A., Z.M.Y., M.Z. and H.E.M.; data curation, A.M.A.; formal analysis, A.M.A., Z.M.Y., M.Z. and H.E.M.; investigation, Z.M.Y. and A.M.A.; methodology, A.M.A.; project administration, Z.M.Y.; resources, A.M.A.; software, A.M.A.; supervision, M.Z. and H.E.M.; validation, A.M.A.; writing—original draft, A.M.A., Z.M.Y., M.Z. and H.E.M.; writing—review and editing, Z.M.Y., A.M.A., M.Z. and H.E.M. All authors have read and agreed to the published version of the manuscript.

Funding: This research received no external funding.

Institutional Review Board Statement: Not applicable.

Informed Consent Statement: Not applicable.

Data Availability Statement: The data are not publicly available due to institutional property rights.

Acknowledgments: This work was supported by the Slovak Research and Development Agency under the Contract no. APVV-20-0281. This work was supported by project of the Ministry of Education of the Slovak Republic VEGA 1/0308/20 Mitigation of hydrological hazards, floods and droughts by exploring extreme hydroclimatic phenomena in river basins.

Conflicts of Interest: The authors declare no conflict of interest.

Appendix A

Table A1. Parameter definitions used for numerical simulation.

Parameter	Definition
H_d	height of subsurface dam measured from the aquifer bottom.
L_d	the distance from the seaside to the subsurface dam location.
H_w	the height from the aquifer bottom to the bottom of the well (Point of abstraction).
L_w	the distance from the subsurface dam to the well location.
D_f	the fracture aperture (conduit diameter).
H_f	the height of fracture aperture measured from the bottom of the aquifer.
Q_w	the abstraction rate of well.

Table A1. Cont.

Parameter	Definition
L_{toe0}	the invasion length (penetration) of the saltwater intrusion of the base scenario case (the Henry problem).
L_{toew}	the invasion length of the saltwater intrusion after installing the subsurface dam.
L_{toefw}	the invasion length of the saltwater intrusion due to the fracture in the subsurface dam and freshwater abstraction
$RE_{w/0}$	the percentage of saltwater penetration decrease due to the subsurface dam construction comparing with the base scenario case of Henry problem: $(L_{toe0} - L_{toew})/L_{toe0}$.
$RE_{afw/0}$	the percentage of saltwater penetration decrease because of the abstraction of freshwater near the fractured subsurface dam compared to the base case: $(L_{toe0} - L_{toefw})/L_{toe0}$.
R	the repulsion ratio of seawater intrusion wedge length
K	the hydraulic conductivity of the aquifer
H	the aquifer depth
ρ_s	the density of saltwater
ρ_f	the density of freshwater
g	the gravity acceleration
n	the porosity of aquifer medium
C_s	the seawater concentration
C_f	the freshwater concentration
ν_s	the viscosity of saltwater
ν_f	the viscosity of freshwater
α_L	the longitudinal dispersivity
α_t	the transversal dispersivity

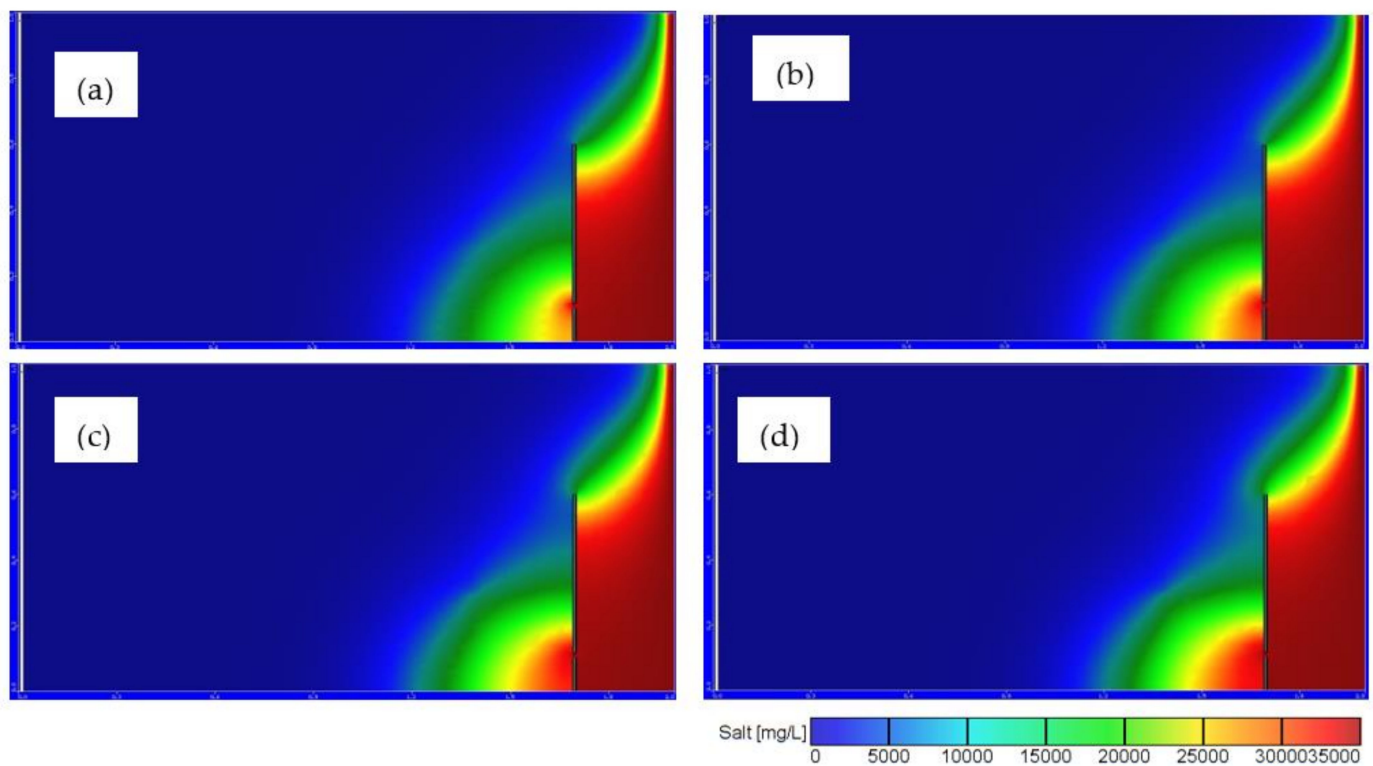


Figure A1. Salinity distribution for $D_f = 0.005$ m, $H_f = 0.1$ m, $L_d = 0.5$ m, $L_w/L_d = 1.0$, for subsurface dam location $L_d = 30$ cm and for different values of abstraction rates: (a) 2×10^{-6} (b) 3×10^{-6} , (c) 4×10^{-6} , and (d) 5×10^{-6} m³/s.

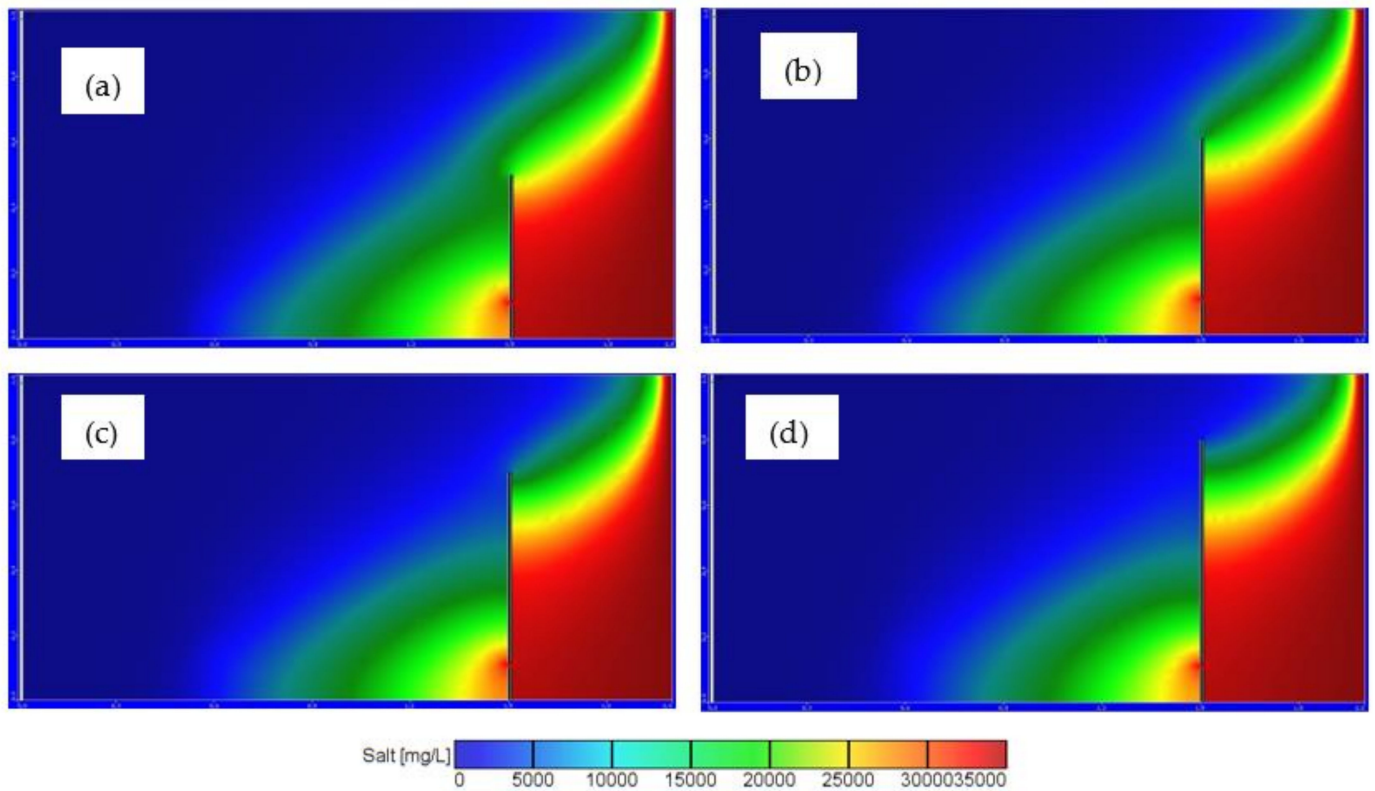


Figure A2. Salinity distribution for $D_f = 0.01$ m, $H_f = 0.1$ m, $L_d = 0.5$ m for different values of subsurface dam heights: (a) 50 cm (b) 60 cm, (c) 70 cm, and (d) 80 cm.

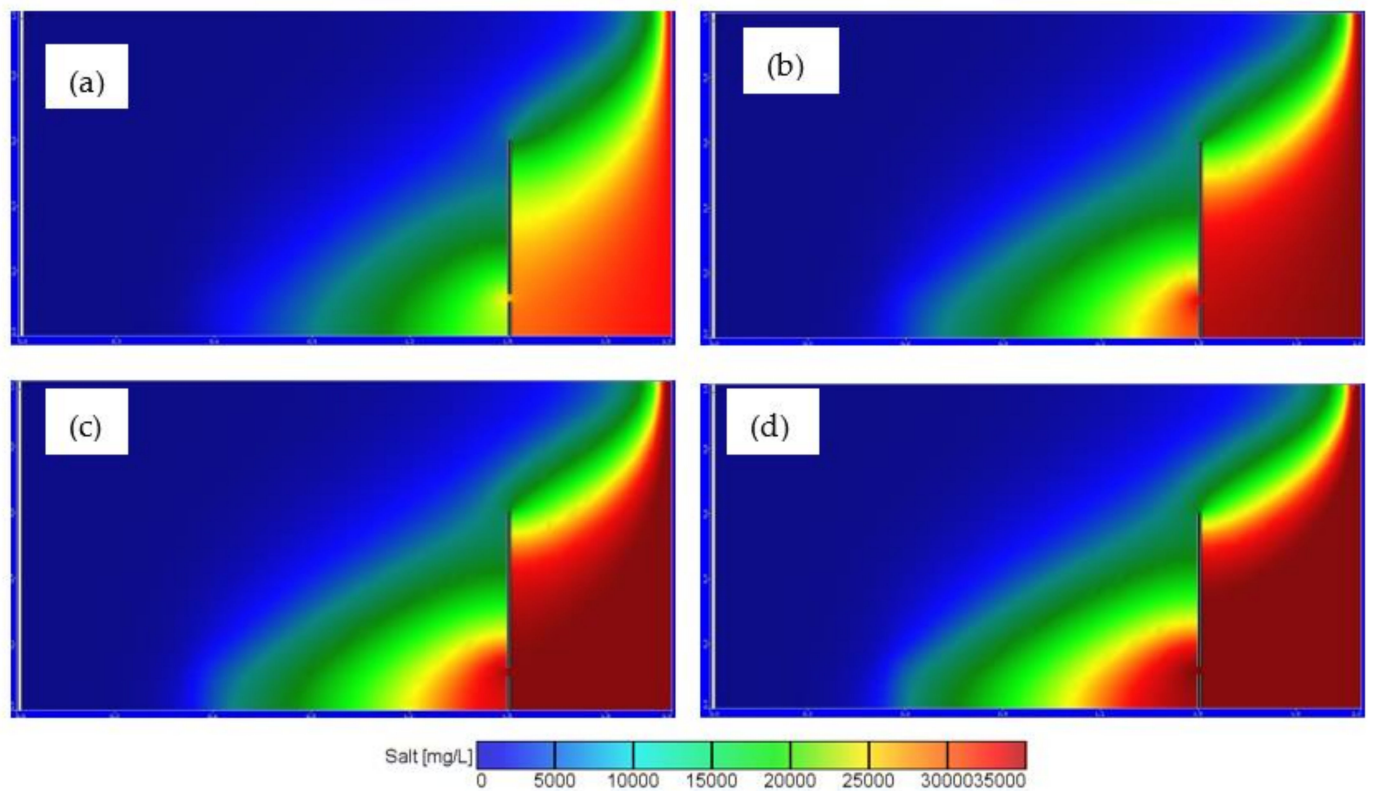


Figure A3. Salinity distribution for $D_f = 0.01$ m, $H_f = 0.1$ m, $L_d = 0.5$ m for different values of saltwater density: (a) 1025 kg/m³ (b) 1025 kg/m³, (c) 1027 kg/m³, (d) 1030 kg/m³.

References

1. Abdoulhalik, A.; Ahmed, A.A. The effectiveness of cutoff walls to control saltwater intrusion in multi-layered coastal aquifers: Experimental and numerical study. *J. Environ. Manag.* **2017**, *199*, 62–73. [[CrossRef](#)] [[PubMed](#)]
2. Cheng, A.H.-D.; Ouazar, D.; Bear, J.; Sorek, S.; Herrera, I. (Eds.) *Seawater Intrusion in Coastal Aquifers—Concepts, Methods and Practices*; Springer: Berlin/Heidelberg, Germany, 1999; ISBN 9780874216561.
3. Kayode, O.T.; Odukoya, A.M.; Adagunodo, T.A.; Adeniji, A.A. Monitoring of seepages around dams using geophysical methods: A brief review. *IOP Conf. Ser. Earth Environ. Sci.* **2018**, *173*, 12026. [[CrossRef](#)]
4. Walther, M.; Graf, T.; Kolditz, O.; Liedl, R.; Post, V. How significant is the slope of the sea-side boundary for modelling seawater intrusion in coastal aquifers? *J. Hydrol.* **2017**, *551*, 648–659. [[CrossRef](#)]
5. Zhang, B.; Zheng, X.; Zheng, T.; Xin, J.; Sui, S.; Zhang, D. The influence of slope collapse on water exchange between a pit lake and a heterogeneous aquifer. *Front. Environ. Sci. Eng.* **2019**, *13*, 20. [[CrossRef](#)]
6. Laabidi, E.; Bouhlila, R. A new technique of seawater intrusion control: Development of geochemical cutoff wall. *Environ. Sci. Pollut. Res.* **2021**, *28*, 41794–41806. [[CrossRef](#)]
7. Abd-Elhamid, H.F.; Abd-Elaty, I.; Negm, A.M. Control of Saltwater Intrusion in Coastal Aquifers. In *The Handbook of Environmental Chemistry*; Springer: Berlin/Heidelberg, Germany, 2018; pp. 355–384.
8. Abdoulhalik, A.; Ahmed, A.; Hamill, G.A. A new physical barrier system for seawater intrusion control. *J. Hydrol.* **2017**, *549*, 416–427. [[CrossRef](#)]
9. Luyun, R.; Momii, K.; Nakagawa, K. Laboratory-scale saltwater behavior due to subsurface cutoff wall. *J. Hydrol.* **2009**, *377*, 227–236. [[CrossRef](#)]
10. Kaleris, V.K.; Ziogas, A.I. The effect of cutoff walls on saltwater intrusion and groundwater extraction in coastal aquifers. *J. Hydrol.* **2013**, *476*, 370–383. [[CrossRef](#)]
11. Anwar, H.O. The effect of a subsurface barrier on the conservation of freshwater in coastal aquifers. *Water Res.* **1983**, *17*, 1257–1265. [[CrossRef](#)]
12. Luyun, R.; Momii, K.; Nakagawa, K. Effects of Recharge Wells and Flow Barriers on Seawater Intrusion. *Ground Water* **2011**, *49*, 239–249. [[CrossRef](#)]
13. Armanuos, A.M.; Ibrahim, M.G.; Mahmud, W.E.; Takemura, J.; Yoshimura, C. Analysing the Combined Effect of Barrier Wall and Freshwater Injection Countermeasures on Controlling Saltwater Intrusion in Unconfined Coastal Aquifer Systems. *Water Resour. Manag.* **2019**, *33*, 1265–1280. [[CrossRef](#)]
14. Chang, Q.; Zheng, T.; Zheng, X.; Zhang, B.; Sun, Q.; Walther, M. Effect of subsurface dams on saltwater intrusion and fresh groundwater discharge. *J. Hydrol.* **2019**, *576*, 508–519. [[CrossRef](#)]
15. Armanuos, A.M.; Al-Ansari, N.; Yaseen, Z.M. Underground Barrier Wall Evaluation for Controlling Saltwater Intrusion in Sloping Unconfined Coastal Aquifers. *Water* **2020**, *12*, 2403. [[CrossRef](#)]
16. Armanuos, A.M.; Al-Ansari, N.; Yaseen, Z.M. Assessing the Effectiveness of Using Recharge Wells for Controlling the Saltwater Intrusion in Unconfined Coastal Aquifers with Sloping Beds: Numerical Study. *Sustainability* **2020**, *12*, 2685. [[CrossRef](#)]
17. Ebeling, P.; Händel, F.; Walther, M. Potential of mixed hydraulic barriers to remediate seawater intrusion. *Sci. Total Environ.* **2019**, *693*, 133478. [[CrossRef](#)]
18. Ozaki, S.; Akl, C.A.; Nagino, T.; Hiroshiro, Y. Investigating Effect of Pumping Ratio on Effectiveness of Barrier Wells for Saltwater Intrusion: Lab-Scale Experiments and Numerical Modeling. *Water* **2021**, *13*, 2100. [[CrossRef](#)]
19. Laabidi, E.; Guellouz, L.; Bouhlila, R. Assessing the Effect of Damaged and Fractured Concrete Cutoff Wall on the Dynamics of Seawater Intrusion. *Water Resour. Manag.* **2021**, *35*, 5367–5381. [[CrossRef](#)]
20. Shiri, N.; Shiri, J.; Yaseen, Z.M.; Kim, S.; Chung, I.M.; Nourani, V.; Zounemat-Kermani, M. Development of artificial intelligence models for well groundwater quality simulation: Different modeling scenarios. *PLoS ONE* **2021**, *16*, e0251510. [[CrossRef](#)]
21. Awadh, S.M.; Al-Mimar, H.; Yaseen, Z.M. Groundwater availability and water demand sustainability over the upper mega aquifers of Arabian Peninsula and west region of Iraq. *Environ. Dev. Sustain.* **2020**, *23*, 1–21. [[CrossRef](#)]
22. Tao, H.; Hameed, M.M.; Marhoon, H.A.; Zounemat-Kermani, M.; Salim, H.; Sungwon, K.; Sulaiman, S.O.; Tan, M.L.; Sa’adi, Z.; Mehr, A.D. Groundwater Level Prediction using Machine Learning Models: A Comprehensive Review. *Neurocomputing* **2022**, *489*, 271–308. [[CrossRef](#)]
23. Rombach, G.A.; Faron, A. Numerical analysis of shear crack propagation in a concrete beam without transverse reinforcement. *Procedia Struct. Integr.* **2019**, *17*, 766–773. [[CrossRef](#)]
24. Hu, M.; Rutqvist, J. Numerical manifold method modeling of coupled processes in fractured geological media at multiple scales. *J. Rock Mech. Geotech. Eng.* **2020**, *12*, 667–681. [[CrossRef](#)]
25. Bennett, M.V.L.; Zheng, X.; Sogin, M.L. The connexin family tree. In *Intercellular Communication through Gap Junctions*; Elsevier: Amsterdam, The Netherlands, 1995; pp. 3–8.
26. Binet, S.; Joigneaux, E.; Pauwels, H.; Albéric, P.; Fléhoc, C.; Bruand, A. Water exchange, mixing and transient storage between a saturated karstic conduit and the surrounding aquifer: Groundwater flow modeling and inputs from stable water isotopes. *J. Hydrol.* **2017**, *544*, 278–289. [[CrossRef](#)]
27. Diersch, H.-J.G. *FEFLOW: Finite Element Modeling of Flow, Mass and Heat Transport in Porous and Fractured Media*; Springer Science & Business Media: Berlin/Heidelberg, Germany, 2013; ISBN 364238739X.